AD-A107 547 GRUMMAN AEROSPACE CORP BETHPAGE NY RESEARCH DEPT F/G 20/4
THE ANALYSIS AND DESIGN OF TWO-ELEMENT AIRFOIL CONFIGURATIONS I--ETC(U)
OCT 81 G VOLPE N00014-75-C-0722
UNCLASSIFIED ONR-CR-215 NL

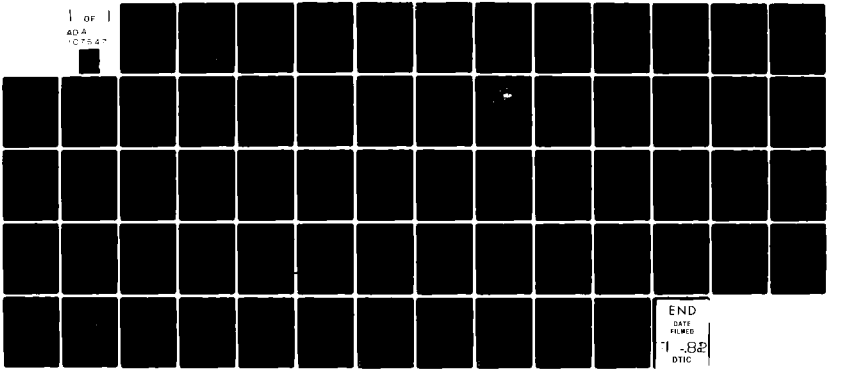

Report ONR CR 215

THE ANALYSIS AND DESIGN OF TWO-ELEMENT AIRFOIL CONFIGURATIONS IN TRANSONIC FLOW

Final Report for Period 19 May 1975 - 30 August 1979

by

G. Volpe

Prepared under Contract N00014-75-C-0722

for

Office of Naval Research
800 North Quincy Street
Arlington, VA 22217

by

Research Department
Grumman Aerospace Corporation
Bethpage, New York 11714

Grumman Research Department Report RE-

THE ANALYSIS AND DESIGN OF TWO-ELEMENT AIRFOIL CONFIGURATIONS IN TRANSONIC FLOW

Final Report for Period 19 May 1975 - 30 August 1979

by

G. Volpe

Prepared under Contract N00014-75-C-0722

ONR Contract Authority ID No. NR215-241/12-31-74(411)

for

Office of Naval Research
800 North Quincy Street
Arlington, VA 22217

by

Research Department
Grumman Aerospace Corporation
Bethpage, New York 11714

October 1981

Approved by Richard A. Scheuing
Richard A. Scheuing
Director of Research

UNCLASSIFIED

SECURITY CLASSIFICATION OF THIS PAGE (When Data Entered)

REPORT DOCUMENTATION PAGE	READ INSTRUCTIONS BEFORE COMPLETING FORM
1. REPORT NUMBER: ONR CR 215 — 2. GOVT ACCESSION NO.: AD-A107 547	3. RECIPIENT'S CATALOG NUMBER:
4. TITLE (and Subtitle): The Analysis and Design of Two-Element Airfoil Configurations in Transonic Flow	5. TYPE OF REPORT & PERIOD COVERED: Final Report 19 May 1975- 30 August 1979
	6. PERFORMING ORG. REPORT NUMBER: RE
7. AUTHOR(s): Giuseppe Volpe	8. CONTRACT OR GRANT NUMBER(s): N00014-75-C-0722
9. PERFORMING ORGANIZATION NAME AND ADDRESS: Grumman Aerospace Corporation, Research Department, Bethpage, New York 11714	10. PROGRAM ELEMENT, PROJECT, TASK AREA & WORK UNIT NUMBERS:
11. CONTROLLING OFFICE NAME AND ADDRESS: Office of Naval Research, 800 North Quincy Street, Arlington, VA 22217	12. REPORT DATE: October 1981
	13. NUMBER OF PAGES: 68
14. MONITORING AGENCY NAME & ADDRESS(if different from Controlling Office)	15. SECURITY CLASS. (of this report): UNCLASSIFIED
	15a. DECLASSIFICATION/DOWNGRADING SCHEDULE:

16. DISTRIBUTION STATEMENT (of this Report)

Approved for public release; distribution unlimited.

17. DISTRIBUTION STATEMENT (of the abstract entered in Block 20, if different from Report)

18. SUPPLEMENTARY NOTES

19. KEY WORDS (Continue on reverse side if necessary and identify by block number)

Transonic Flow, Two-Element Airfoil Systems, Slats, Flaps, Viscous Flow, Airfoil Design

20. ABSTRACT (Continue on reverse side if necessary and identify by block number)

This report describes the development of numerical techniques for predicting the flow over two-element airfoil configurations, such as airfoils with a slat or a flap, at transonic speeds and for designing such airfoil systems. The effort was divided in three phases. The first phase involved the development of a method to compute the inviscid flow over these configurations. In the second phase the inviscid code was coupled to a boundary layer calculation program in order to compute the loss in performance

DD FORM 1 JAN 73 1473 EDITION OF 1 NOV 65 IS OBSOLETE S/N 0102-014-6601

UNCLASSIFIED

SECURITY CLASSIFICATION OF THIS PAGE (When Data Entered)

due to viscous effects. In the third phase an inverse design code that constructs the airfoil system corresponding to a desired pressure distribution was developed.

ABSTRACT

This report decribes the development of numerical techniques for predicting the flow over two-element airfoil configurations, such as airfoils with a slat or a flap, at transonic speeds and for designing such airfoil systems. The effort was divided in three phases. The first phase involved the development of a method to compute the inviscid flow over these configurations. In the second phase the inviscid code was coupled to a boundary layer calculation program in order to compute the loss in performance due to viscous effects. In the third phase an inverse design code that constructs the airfoil system corresponding to a desired pressure distribution was developed.

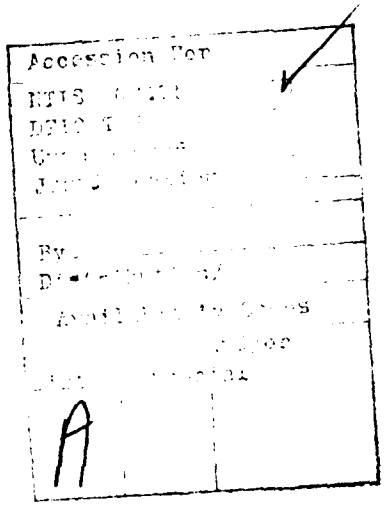

CONTENTS

Section		Page
1	Introduction	1
2	The Inviscid Flow Over Two-Element Airfoils	5
	2.1 Results of Inviscid Analysis	9
3	The Viscous Flow Over Two-Element Systems	21
	3.1 Boundary Layer Calculation	21
	3.2 Coupling of Inviscid Flow and Boundary Layer	23
	3.3 Viscous Flow Computations	24
4	The Inverse Design Problem	35
	4.1 Full Design Formulation	36
	4.2 Mixed Design	38
	4.3 Examples of Inverse Design	39
5	Discussion and Conclusion	53
6	References	57

ILLUSTRATIONS

Figure		Page
1	Sequence of Conformal Mappings.	6
2	Coordinate Grid in Annular Domain and Sweep Directions.	11
3	Coordinate Grid in Physical Domain: Clark Y Airfoil With 30% Maxwell Slat, 10% Gap	11
4	Computed Surface Pressure Distribution: Clark Y Airfoil With 30% Maxwell Slat; $M_\infty = 0.65$, $\alpha = 6°$	12
5	Computed Streamlines in Physical Domain Clark Y Airfoil With 30% Maxwell Slat; $M_\infty = 0.65$, $\alpha = 6°$	13
6	Computed Streamlines in an Annular Domain Clark Y Airfoil With 30% Maxwell Slat; $M_\infty = 0.65$, $\alpha = 6°$	14
7	Computed Pressure Distribution NACA 23012 Airfoil With 2H Flap, $M_\infty = 0.5$, $\alpha = 4°$.	15
8	Mach Number Contours: NACA 23012 Airfoil With 2H Flap, $M_\infty = 0.5$, $\alpha = 4°$.	16
9	Computed and Experimental Surface Pressures on a CCW Airfoil With 25° Slat; $M_\infty = 0.1$, $\alpha = 12°$, $C_\mu = 0$.	17
10	Computed Streamlines, CCW Airfoil With 25° Slat; $M_\infty = 0.1$, $\alpha = 4.6°$, $C_\mu = 0.1285$	18
11	Computed and Experimental Surface Pressures On a CCW Airfoil With 25° Slat; $M_\infty = 0.1$, $\alpha = 4.6°$, $C_\mu = .1285$	19
12	Computed and Experimental Surface Pressure Distributions: NACA $M_\infty = 0.133$, $\alpha = 0°$, $Re = 3.5 \times 10^6$.	25
13	Computed and Experimental Surface Pressure Distribution: NACA 64A010 Airfoil With 18A Slat; $M_\infty = 0.7$, $\alpha = 6°$, $Re = 7.8 \times 10^6$.	26
14	Computed and Experimental Surface Pressure Distributions: NACA 64A406 Airfoil With 7.8A Slat; $M_\infty = 0.649$, $\alpha = 4.6°$, $Re = 2.0 \times 10^7$.	28
15	Computed Mach Number Contours: NACA 64A406 Airfoil With 7.8A Slat; $M_\infty = 0.649$, $\alpha = 4.6°$, $Re = 2.0 \times 10^7$.	29
16	Computed and Experimental Pressure Distributions: NACA 64A406 Airfoil With a 7.8F Slat; $M_\infty = 0.649$, $\alpha = 6.5°$, $Re = 2.0 \times 10^7$.	30

Figure		Page
17	Computed Mach Number Contours: NACA 64A406 Airfoil With 7.8F Slat; $M_\infty = 0.649$, $\alpha = 6.5°$, $Re = 2.0 \times 10^7$	31
18	Computed and Experimental Surface Pressure Distributions: NACA 64A406 Airfoil With 10.6C Slat; $M_\infty = 0.649$, $\alpha = 6.5°$, $Re = 2.0 \times 10^7$	32
19	Computed and Experimental Pressure Distributions: Supercritical Airfoil One, $M_\infty = 0.70$, $\alpha = -1.74°$, $Re = 10^7$	33
20	Computed Pressure Distribution on Modified NACA 64A408 Airfoil With Slat; $M_\infty = 0.6$, $\alpha = 6°$	40
21	Mach Number Contours on Modified NACA 64A408 Airfoil with Slat; $M_\infty = 0.6$, $\alpha = 6°$	41
22	Airfoil/Slat System After One Design Cycle; Main Airfoil Only Modified; $M_\infty = 0.6$	41
23	Pressure Distribution Computed on Airfoil/Slat System Constructed After One Design Cycle; $M_\infty = 0.6$	42
24	Pressure Distribution Computed on Airfoil/Slat System Attained After Three Design Cycles; $M_\infty = 0.6$	43
25	Airfoil/Slat System Attained After Three Design Cycles; Main Airfoil Only Modified; $M_\infty = 0.6$	44
26	Computed Pressure Distribution on NACA 23012 Airfoil with 2H Flap; $M_\infty = 0.55$, $\alpha = 0°$	45
27	Mach Number Contours on NACA 23012 Airfoil with 2H Flap; $M_\infty = 0.55$, $\alpha = 0°$	47
28	Airfoil/Flap System After One Design Cycle; Main Airfoil Only Modified; $M_\infty = 0.55$	47
29	Pressure Distribution Computed on Airfoil with Flap System Constructed After One Design Cycle; Main Airfoil Only Modified; $M_\infty = 0.55$	48
30	Airfoil with Flap System After One Design Cycle; Both Airfoil Elements Modified; $M_\infty = 0.55$	48
31	Pressure Distribution Computed on Airfoil with Flap System Constructed After One Design Cycle; Both Airfoil Elements Modified; $M_\infty = 0.55$	49
32	Pressure Distribution Computed on Airfoil with Flap System Attained After Four Design Cycles; Both Elements Modified; $M_\infty = 0.55$	50

Figure		Page
33	Airfoil with Flap System Attained After Four Design Cycles; Both Airfoil Elements Modified; $M_\infty = 0.55$	51
34	Summary of Flap Geometry.	51

LIST OF SYMBOLS

a	local speed of sound
c_f	skin friction coefficient
C_L	lift coefficient
C_p	pressure coefficient
C_μ	blowing coefficient on CCW airfoil
E_1	defined by Eq (9)
E_2	defined by Eq (9)
f	defined by Eq (2)
G	reduced potential
$\tilde{H}$	metric of conformal mappings
H	reduced metric
k, k_1, K_2	mapping constants
L	defined by Eq (8)
M	Mach number
Re	Reynolds number
r_∞	radial direction in annular domain
r_s	radius of inner ring corresponding to secondary airfoil in annular domain
r	radius of point of infinity in annular domain
s	local streamwise coordinate
u	velocity component in θ direction
v_s	surface source distribution
v	velocity component in r direction
x,y	cartesian coordinates in physical plane
z	physical domain = $x + iy$

α	angle of attack
β	defined by Eq (6)
γ	ratio of specific heats
Γ_1, Γ_2	circulation constants for main and secondary airfoils
δ	airfoil coordinate change normal to the surface
δ^*	displacement thickness
ζ	complex annular domain, $= re^{i\theta}$
θ	azimuthal direction in annular domain
ϕ	complete potential function
ϕ_1	free stream contribution to potential
ϕ_2	circulatory flow contribution to potential
ρ	density

Subscripts

o	value at airfoil surface
e	value at edge of boundary layer
∞	free stream quantity

1. INTRODUCTION

Modern aircraft designs with primary mission requirements in the supersonic or subsonic speed regimes often are also required to maneuver effectively at transonic speeds. This can be achieved if high lift coefficients can be generated without incurring excessive drag or buffet at transonic speeds. This conflicts somewhat with the requirements for airfoils that are designed for efficient cruise at low lift coefficients. However, it has been demonstrated in tests on modern fighter aircraft that these conflicting requirements can be reconciled by the deployment of mechanical high lift devices at the maneuver condition. The installation of leading edge slats on the F-4 aircraft and the deployment of the existing slat on the F-14 in flight have shown significant improvements in the transonic maneuvering the performance of these aircraft. Although these flight experiments have clearly demonstrated the usefulness of leading edge slats for transonic maneuvering, the paucity of experimental data currently makes it difficult to determine what can be achieved with these maneuvering devices. An experimental study on such configurations would be extremely expensive in light of the large number of configurations that need be tested and the high speeds and Reynolds numbers required in a meaningful wind tunnel test program. A theoretical tool for the analysis of the transonic flow over two-element airfoil systems would be a valuable first step in aiding the designer by reducing the number of configurations that need be tested and by providing insight into the flow phenomena that are present at high speeds.

This report describes the development of a method for computing the inviscid and viscous transonic flow over an airfoil with a leading-edge slat or a trailing-edge flap. Numerical methods are described for solutions to both the direct and inverse design problems. The description of the method will be brief as details of the work have already been reported in Ref 1-4. This report is essentially a summary of the work reported in these references with emphasis given to examples of computed results.

The methods described in this report are applicable to general two-element airfoil systems, employing either a single slat or flap. In general, even the inviscid flow over these configurations is difficult to

obtain analytically because of the complicated geometry of the multi-connected domain. Small disturbance approximations (such as that used for this problem in Ref 5) are not adequate since the interaction of the flow between the airfoils will in general lead to very large perturbations to the flow field.

Mixed flow relaxation techniques, following the work of Murman and Cole (Ref 6), are applied to compute the flow about an airfoil with a slat or a flap at transonic speeds. The approach, as discussed in Ref 1 and 2 and summarized in Section 2, is to solve the full inviscid, irrotational flow equations about two-element airfoil systems. The methodology consists of 1) the development of a suitable computational plane and grid system, 2) the evaluation of an appropriate set of governing inviscid equations and boundary conditions in terms of smoothly varying, single-valued functions in the computational domain, and 3) the establishment of a stable and accurate numerical procedure for the solution of the governing equations.

At high Reynolds numbers, solutions of the inviscid flow equations provide a reasonable estimate of the lift on an airfoil, provided the angle of attack is below that for maximum lift. However, inviscid theory provides no information on skin friction, form drag, or maximum lift of an airfoil. These important characteristics are completely dominated by effects due to boundary layer growth on both airfoil surfaces. For standard airfoils at low speeds, boundary layer effects are relatively weak at high Reynolds number and can be treated as a small correction to the inviscid solution. In transonic flows over supercritical airfoils and multi-element airfoil systems, the situation is much more severe, with viscous effects playing a significant role in reducing the lift from inviscid values.

Our approach to computing viscous effects on two-element airfoil systems is based on interacting boundary layer theory with the inviscid and viscous flows solved simultaneously in a self-consistent fashion, by iteration. The development of the boundary layer over the surfaces of the airfoils is computed with methods based on a turbulent kinetic energy formulation and is coupled to the inviscid flow using surface source flow boundary conditions. The effect of the boundary layer on the inviscid flow, and in particular, on the circulation, will be felt through the boundary conditions involving the equivalent surface sources. In our analysis we assume that the airfoil elements are sufficiently far apart so that the boundary layers do not merge

in the slot region. To account for strong interaction regions near the airfoil trailing edges and in the vicinity of shock waves, semi-empirical smoothing procedures are used. Although a rational analytic approach to the trailing edge interaction has been proposed by Melnik, Chow and Mead (Ref 7), it has proved too complicated to implement into our approach at the present. Most available data on two-element airfoil systems at transonic speeds indicate substantial regions of flow separation. In the absence of a definitive theoretical method for treating turbulent separated flows, we resort to a semi-empirical procedure to model this phenomena. Details of our viscous flow method are given in Section 3.

We applied our method to several typical slatted and flapped airfoil configurations and have compared the results with existing wind tunnel test data. A discussion of these results is presented in Section 3. This section also contains a theoretical study of a typical fighter aircraft slat system to demonstrate how such a study can be used to supplement and even partially replace expensive experimental investigations. Used in such fashion the analysis program becomes useful as a tool for designing transonic maneuvering systems because for the first time it provides some insight into the complicated flow fields that are set up when two closely spaced airfoil elements operate at high speeds.

An even more valuable tool for the design of two-element airfoil systems is the numerical solution of the inverse problem where the configuration required to produce a desired pressure distribution over either or both elements, or parts of them, is constructed. In Ref 8 the inverse problem for two- (and multi-) element airfoil systems has been addressed for the case of incompresible flows. Section 4 describes a method for generating the two-element airfoil configuration corresponding to a desired pressure distribution at supercritical speeds. The design of the configuration is achieved through sequential modifications of a pair of initial profiles. The required modifications are arrived at by the numerical solution of the flow field about the current profiles with Dirichlet-type boundary conditions. Both the full design problem, where the entire configuration is to be constructed, and the mixed design problem, where only one of the airfoils or segments of either are to be altered, are discussed. Several design cases are presented in Section 4. In Section 5 recommendations for further research in both the analysis and design problems are discussed.

2. THE INVISCID FLOW OVER TWO-ELEMENT AIRFOILS

The methodology employed in the computation of the inviscid flow over two-element airfoil systems has been described in previous reports (Ref 1-4); only a brief summary will be given here. The first step is to transform the infinite domain about the airfoils into a finite one where the surface and far-field boundary conditions can be satisfied more easily. A suitable computational space for the doubly connected physical domain of a two-element configuration $z = x + iy$ in cartesian coordinates, is obtained by mapping this into an annulus, $\zeta = re^{i\theta}$, r and θ being the polar coordinates. The transformation itself follows from the work of Ives (Ref 9), and it is the result of five sequential mappings. The first, a Karman-Trefftz transformation, removes the corner at the trailing edge of the main airfoil and opens this up into a near circle. The second, a numerical mapping, converts the near circle into a perfect one. Then the second airfoil is opened up into a near circle by an analytic removal of its trailing edge corner, and subsequently its geometric center is transferred to the center of the circle representing the main airfoil. In the last step the near circle representing the second airfoil is mapped into a circle. The last three mappings are constructed in a way that retains the shape of the first circle. The five mappings are all conformal and with this transformation the entire physical space is mapped into the annular region between two circles with infinity becoming a single point between them. The mapping sequence is illustrated in Fig. 1.

The governing equations for the inviscid, irrotational compressible flow are written in the computational domain using the metric of the mapping. By the introduction of a potential function, ϕ, the number of equations is reduced to one. The mapping introduces several singularities in the equation for the potential, but since the mapping is analytic and the transformation is known everywhere, the singularities can be removed analytically. Near infinity ($\zeta = r_\infty$) the metric of the mapping, $H = \left|\frac{dz}{d\zeta}\right|$, behaves as $\frac{K}{(\zeta - r_\infty)^2}$ where k is a complex constant ($K_1 e^{iK_2}$). The metric is normalized by its behavior at infinity so that a smooth bounded function

$$\tilde{H} = \frac{f}{K_1} H \qquad (1)$$

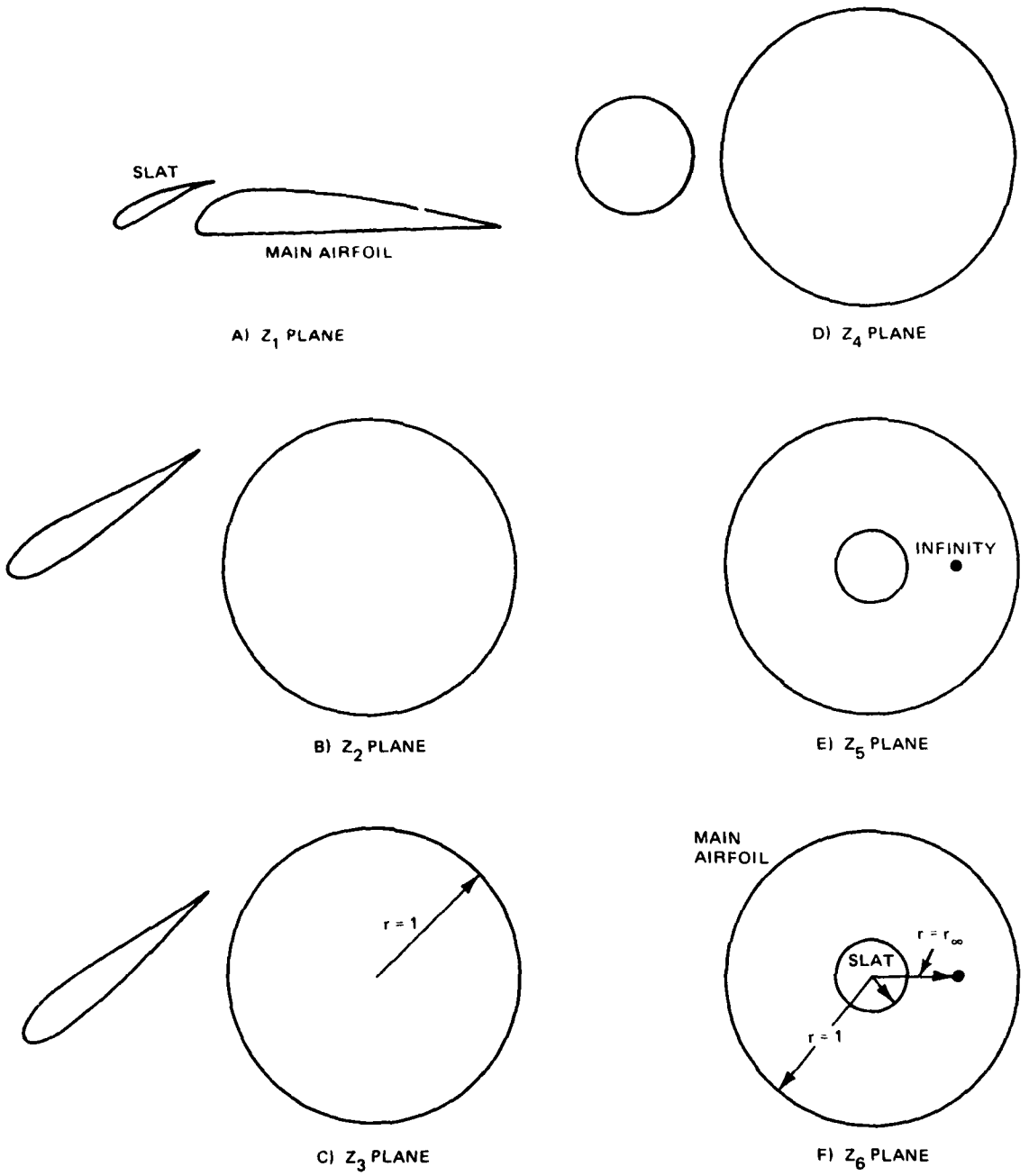

0737-001(T)

Fig. 1 Sequence of Conformal Mappings

results. Here

$$f = |\zeta - r_\infty^2| = r^2 - 2rr_\infty \cos\theta + r_\infty^2 \tag{2}$$

A single-valued, continuous reduced potential function, G, can be defined by subtracting terms corresponding to the free stream and circulatory flows around each element from the full potential. Thus,

$$G = \Phi - \Phi_1 - \Phi_2 \tag{3}$$

where

$$\Phi_1 = -\frac{K_1}{f}\left[r\cos(\theta+\alpha - K_2) - r_\infty \cos(\alpha - K_2)\right] \tag{4}$$

$$\Phi_2 = -(\Gamma_1 + \Gamma_2)\tan^{-1}\left[\sqrt{1-M_\infty^2}\,\tan\beta\right] - \Gamma_2\theta \tag{5}$$

and

$$\beta = K_2 - \alpha + \pi - \tan^{-1}\left[\frac{r\sin\theta}{r\cos\theta - r_\infty}\right] \tag{6}$$

M_∞ is the free stream Mach number and Γ_1 and Γ_2 are the circulation constants about the main and secondary airfoils, respectively. With u and v as the velocity components along the coordinate lines and the local speed of sound, a, the equation governing the flow can now be written as:

$$\begin{aligned}&(a^2-v^2)fG_{rr} - 2uv\left[\frac{1}{r}G_{r\theta} - \frac{1}{r^2}(G_\theta - \Gamma_2)\right]\\ &+ (a^2-u^2)f\left(\frac{1}{r^2}G_{\theta\theta} + \frac{1}{r}G_r\right) + (u^2+v^2)K_1\left(v\tilde{H}_r + \frac{u}{r}\tilde{H}_\theta\right) + L = 0\end{aligned} \tag{7}$$

where

$$\begin{aligned}L = &-\frac{4uv}{r}\left[(r-r_\infty\cos\theta)(G_\theta-\Gamma_2) + r^2 r_\infty \sin\theta\, G_r\right]\\ &+ 2(u^2+v^2)\left[(r-r_\infty\cos\theta)G_r - \frac{r_\infty}{r}\sin\theta(G_\theta-\Gamma_2)\right]\end{aligned} \tag{8}$$

$$-(\Gamma_1 + \Gamma_2)\ \frac{E_1}{f}\Big\{ 2(u^2-v^2)(r-r_\infty\cos\theta)r_\infty\sin\theta$$

$$+ 2\,uv\,(f-2r_\infty^2\sin^2\theta)-E_2[a^2f-(vr_\infty\sin\theta - ur + ur_\infty\cos\theta)^2]\Big\} \qquad \begin{matrix}(8)\\(\text{contd})\end{matrix}$$

and

$$E_1 = \frac{\sqrt{1-M_\infty^2}}{1-M_\infty^2\sin^2\beta}\ , \qquad E_2 = \frac{-M_\infty^2\sin 2\beta}{1-M_\infty^2\sin^2\beta} \qquad (9)$$

Also

$$a^2 = \frac{1}{M_\infty^2} + \left(\frac{\gamma-1}{2}\right)(1-u^2-v^2) \qquad (10)$$

where γ is the ratio of specific heats.

The equation is of mixed type and it is solved by replacing it by its finite difference analog at the nodes of a suitable grid in the computational plane. In the annulus a simple polar coordinate system emanating from the center automatically generates an orthogonal grid in which both airfoils lie along grid lines. An accurate application of the boundary conditions is then made in a relatively straightforward manner. The boundary conditions are that the normal component of velocity be zero at each surface

$$v = 0 \quad \text{or} \quad r = 1 \text{ and } r = r_s \qquad (11)$$

The finite difference analog of this equation is generated by introducing "dummy" grid lines beyond each surface grid line. As described in Ref 2, an additional stretching is used to concentrate grid points near the leading and trailing edges of both elements and to place both trailing edge points and the point of infinity at grid nodes.

The numerical procedure employs standard relaxation techniques along with a nonconservative, type-dependent, rotated difference scheme. To make sure that the field is never swept at more than 90° from the streamline direction, the computational domain is divided into four regions using the ring going through the infinity point, as shown in Fig. 2, and then the region over each of the airfoil surfaces is swept from the leading edge to the trailing edge. Fig. 3 shows a typical computational grid as it appears in the physical plane. This procedure leads to a high level of concentration of mesh points is obtained near the leading and trailing edges and in the gap.

A good set of initial conditions for the reduced potential to start the iteration process is given by the incompressible solution for the flow over two circles which can be written in closed form as a series. At the end of each iteration sweep the two circulation constants, Γ_1 and Γ_2, are evaluated by applying the Kutta condition at each trailing edge.

2.1 RESULTS OF INVISCID ANALYSIS

The variety of two-element configurations that can be analyzed by the method is illustrated in Fig. 3 through 11. The configuration shown in Fig. 3, together with a representation of the computational grid as it appears in the physical plane, is a Clark Y airfoil with a 30% Maxwell slat, and the pressure distributions computed for a Mach number of 0.6 and an angle of attack of 6° are given in Fig. 4. The angle of attack is the angle between the airfoil's reference line and the free stream direction. The figures show very large supersonic regions can be seen to be present on both elements. These are more evident in Fig. 5, which shows the sonic lines along with some computed streamlines. Figure 6 gives the streamline pattern and the supersonic regions as they appear in the annular domain. Figures 7 and 8 give the computed pressure distribution and Mach number contours for an airfoil-flap arrangement.

Transonic data for two-element airfoil systems are scarce, and there are little data at any speed where viscous effects are negligible. However, data recently made available by the David Taylor Research and Development Center have made possible the verification of the results of the method. The airfoil-slat combination shown in Fig. 9 was designed for low-speed application on a circulation control wing. The unconventional back end of the main airfoil was designed to operate as a Coanda jet. A jet of high velocity

air is ejected tangentially along the upper surface near the trailing edge of the main airfoil. The jet wraps around the rounded trailing edge entraining the outer flow. The result is an airfoil system with a very high circulation. The slat is deployed to prevent flow separation near the leading edge of the main component. The case shown in Fig. 9 is for a low Mach number, an angle of attack of 12°, and zero blowing. Because of the small amount of aft loading, viscous effects on the main airfoil are small; because of the high angle of attack, there is very little separation on the slat. As a result there is very good agreement between the computations and the experimental data. Leading edge expansions are predicted correctly on both elements. The only discrepancy is on the lower surface of the slat where a small separation bubble is likely to exist. The lift coefficient on this configuration is 1.83.

Blowing can be simulated in the computational method by adjusting the positon of the stagnation point on the main airfoil, as seen in Fig. 10. The location itself is chosen to match the circulation around the main airfoil. The streamline pattern in Fig. 10 has been computed for an angle of attack of 4.6° and a moderate amount of blowing. In this case the slat is practically aligned with the oncoming flow. The computed pressure coefficient distribution and the experimental data are compared in Fig. 11. Agreement in this case is even better. Now there is no flow separation on the lower surface of the slat, and there is good agreement in this region also. Leading edge peaks are correctly predicted and the large expansion near the trailing edge of the main component corresponding to the Coanda jet is also in agreement. The lift coefficient in this case is 4.70. It should be mentioned that because of the rounded trailing edge of the main airfoil, a slight modification of the first mapping step was necessary. Since there are no corners on this airfoil element, the rear singular point appearing in the mapping is placed inside the airfoil rather than on the trailing edge itself.

The reduced importance of viscous effects on the last configuration has made it possible to test the accuracy of the inviscid analysis program. The absence of such phenomena is unusual, however, and an accurate prediction method should account for the effects on performance due to boundary layer growth on the airfoil surfaces.

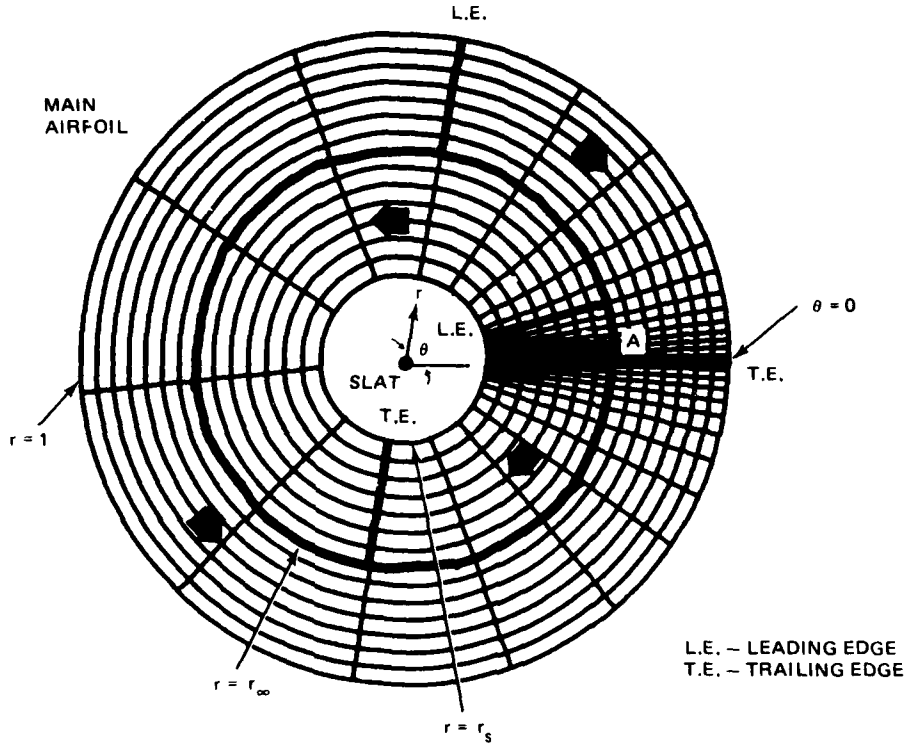

0737-002(T)

Fig. 2 Coordinate Grid in Annular Domain and Sweep Directions

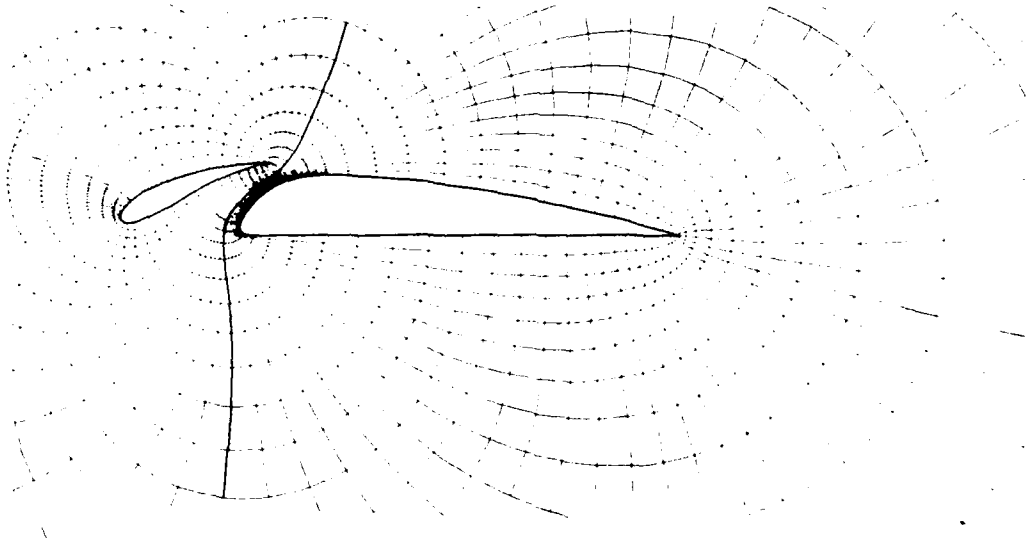

0737-003(T)

Fig. 3 Coordinate Grid in Physical Domain: Clark Y Airfoil With 30% Maxwell Slat, 10% Gap

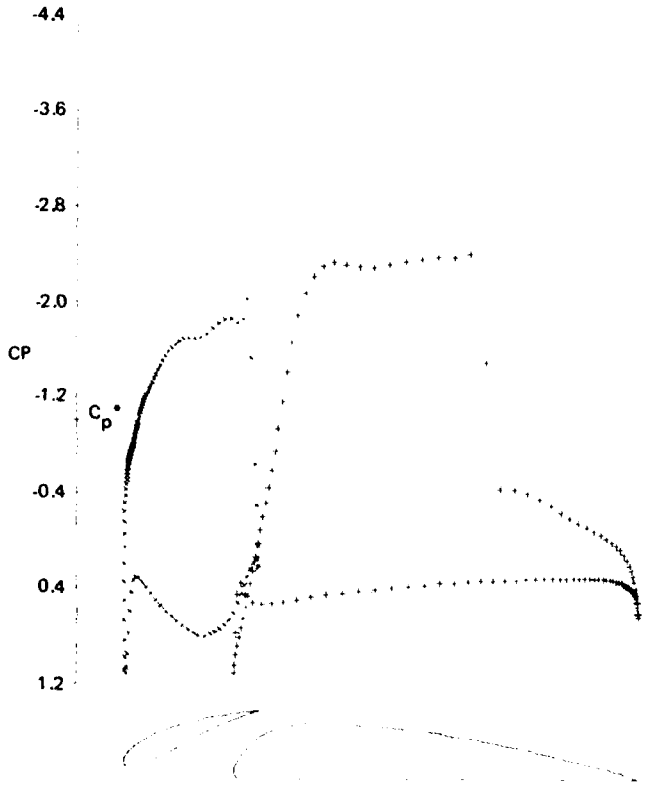

0737-004(T)

Fig. 4 Computed Surface Pressure Distribution: Clark Y Airfoil With 30% Maxwell Slat; $M_\infty = 0.65$, $\alpha = 6^\circ$

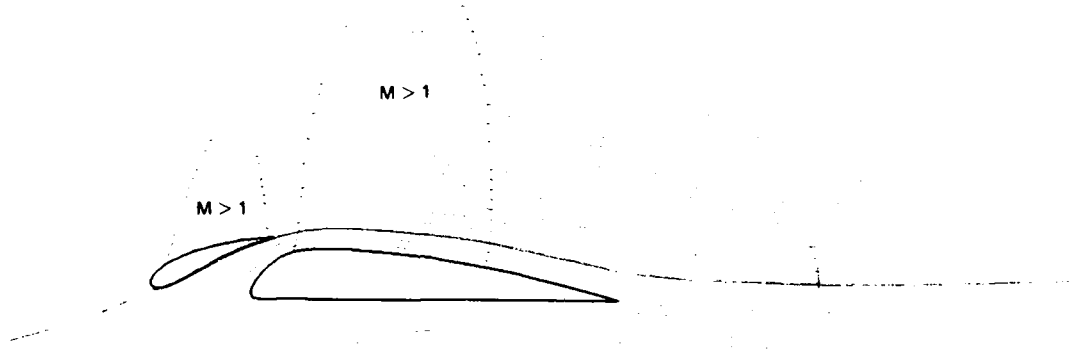

0737-005(T)

Fig. 5 Computed Streamlines in Physical Domain Clark Y Airfoil With 30% Maxwell Slat, $M_\infty = 0.65$, $\alpha = 6^\circ$

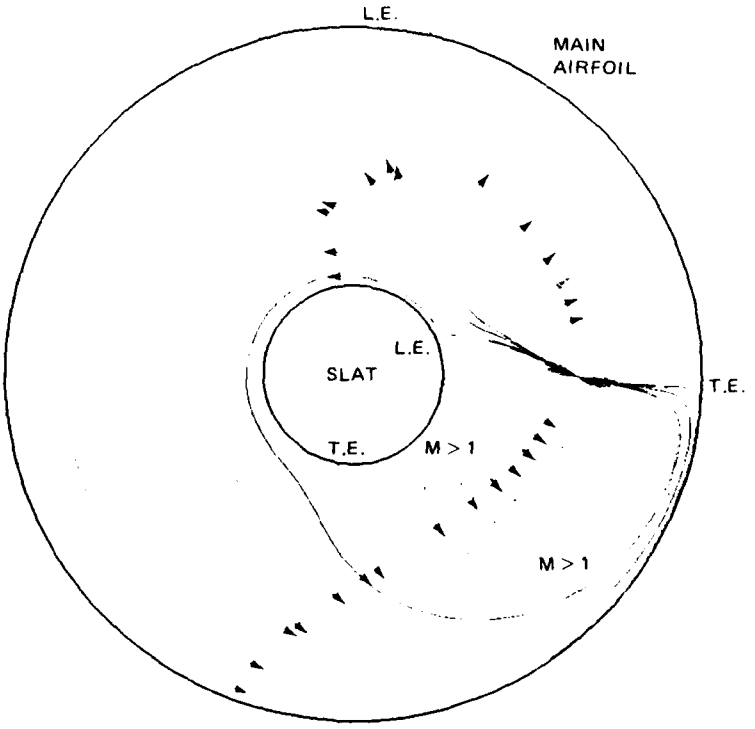

0737-006(T)

Fig. 6 Computed Streamlines in Annular Domain Clark Y Airfoil With 30% Maxwell Slat; $M_\infty = 0.65$, $\alpha = 6^\circ$

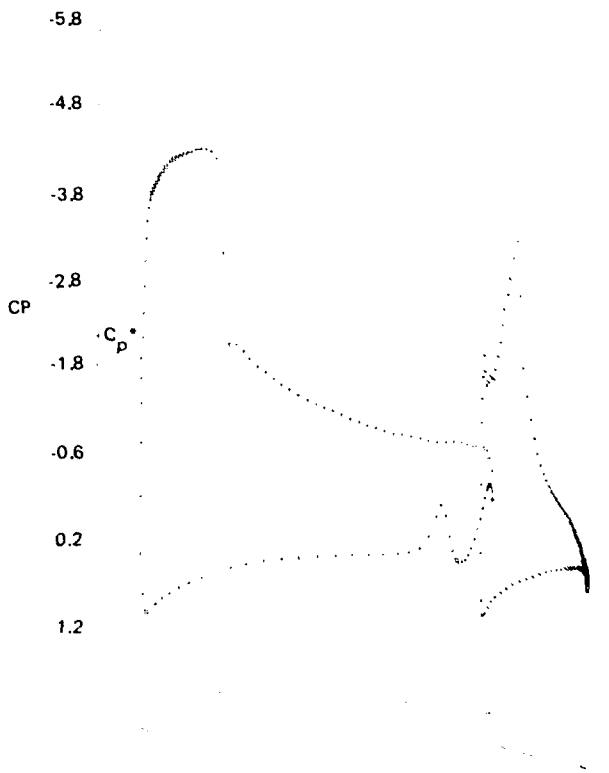

0737-007(T)

Fig. 7 Computed Pressure Distribution NACA 23012 Airfoil With 2H Flap, $M_\infty = 0.5$, $\alpha = 4^\circ$

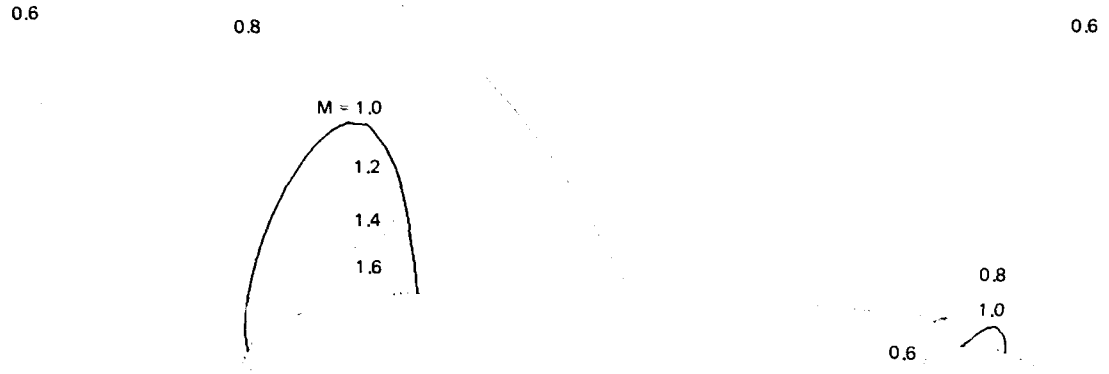

0737-008(T)

Fig. 8 Mach Number Contours:
NACA 23012 Airfoil With 2H Flap, $M_\infty = 0.5$, $\alpha = 4^\circ$

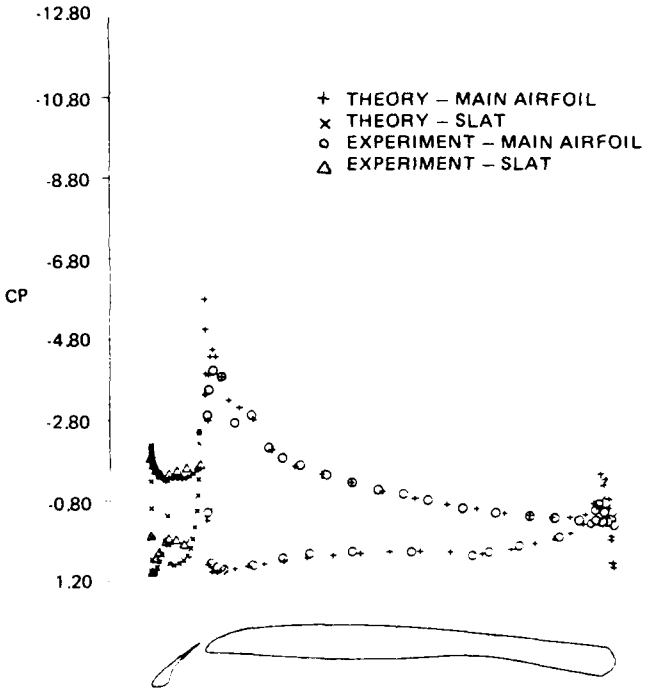

0737-009(T)

Fig. 9 Computed and Experimental Surface Pressures on a CCW Airfoil With 25° Slat – $M_\infty = 0.1$, $\alpha = 12^\circ$, $C_\mu = 0$

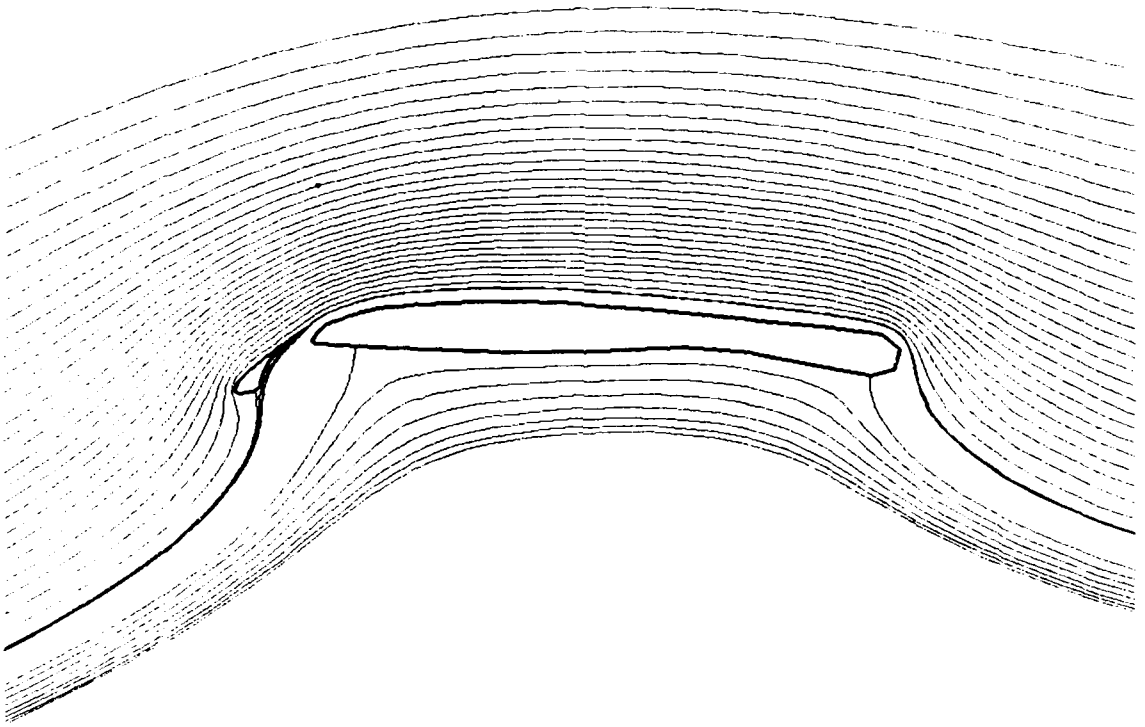

0737-011(T)

Fig. 10 Computed Streamlines, CCW Airfoil With 25° Slat, $M_\infty = 0.1$, $\alpha = 4.6°$, $C\mu = 0.1285$

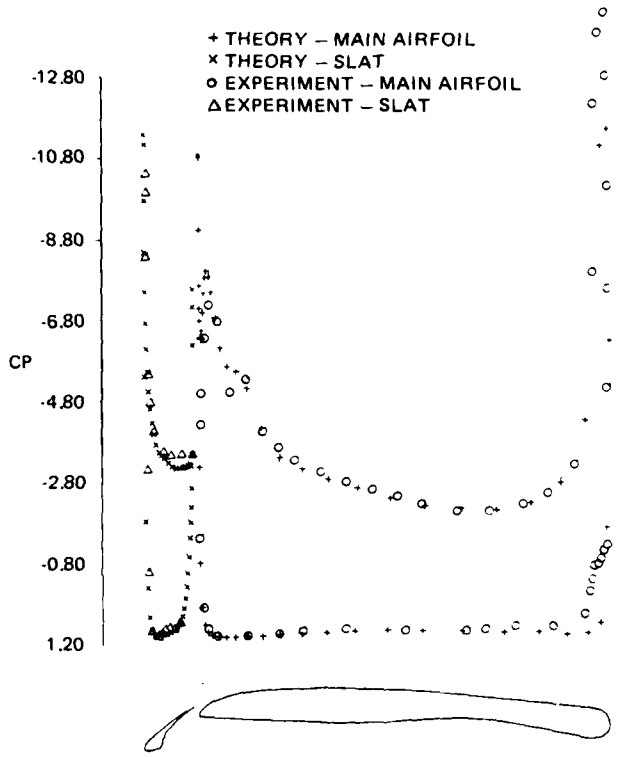

0737-010(T)

Fig. 11 Computed and Experimental Surface Pressures On a CCW Airfoil With 25° Slat – $M_\infty = 0.1$, $\alpha = 4.6°$, $C_\mu = .1285$

3. THE VISCOUS FLOW OVER TWO-ELEMENT SYSTEMS

3.1 BOUNDARY LAYER CALCULATION

The development of the airfoil boundary layer is assumed to be driven by the inviscid flow with equivalent surface sources. At transonic speeds the growth of the boundary layers on the upper and lower surfaces of an airfoil is highly unsymmetrical. High aft-loadings cause a rapid thickening on the upper surface of the airfoil and a thinning on the lower surface as the trailing edge is approached. The net effect is to produce a strong uncambering of the "equivalent" airfoil shape, which leads to a sharp reduction in lift. This uncambering effect could also be looked at as a strong upwash at the rear of the airfoil. In the present method the effect of the boundary layer on the inviscid flow, and the circulation in particular, will be felt through the updated computation with the equivalent source strength on the airfoil surface. It is assumed that gap sizes are large enough so that the boundary layers of neighboring surfaces do not merge. In addition, the effect of a finite thickness wake passing over the downstream element is ignored. In light of the practical sizes of slats for transonic applications these assumptions are not unreasonable.

The growth of the laminar boundary layer over the forward portion of the airfoil is computed using an integral method based on the approach of Thwaites (Ref 10). At transonic speeds the laminar run on an airfoil surface is usually quite short, and it was felt that sufficient accuracy would be obtained with an integral method. The particular formulation employed is that described by Rott and Crabtree (Ref 11) who, by the use of the Illingworth-Stewartson transformation, showed how the compressible laminar flow on a surface is reduced to an equivalent incompressible flow that can be computed by Thwaites' original method. Transition from laminar to turbulent flow is still an imperfectly understood phenomenon and difficult to predict. Several empirical criteria, such as Crabtree's and Michel's both, reported in Ref 12, are available. Alternatively, the point of transition can be specified in the computational method. Since transition is most often fixed in wind tunnel tests, this feature is extremely useful. In addition, should laminar separation be predicted the transition point is fixed at the laminar

separation point and the computation is continued as a turbulent boundary layer. Transition is assumed to occur instantaneously, and from this point on the turbulent boundary layer solution is obtained with either Bradshaw's finite difference method (Ref 13) or Green's lag entrainment method (Ref 14). Starting conditions for the turbulent calculation are obtained by requiring continuity of the mass and momentum fluxes within the boundary layer during transition. Bradshaw's method integrates numerically along the surface three equations: the mean motion equations for continuity and momentum and an empirical equation for the shear stress obtained from the exact turbulent energy equation. Since the three equations are of a hyperbolic nature, the integration is performed by marching along the surface. This method has been shown to be very accurate for a wide variety of flows. Green's method solves at each station along the surface a system of three equations: the momentum integral equation, an entrainment equation, and an equation for the streamwise rate of change of the entrainment coefficient. The last of these equations was developed from Bradshaw's empirical equation for the shear stress. Thus the two methods have the same physical foundations, and the results of the two methods agree very well and produce essentially the same results in the program. Both methods are included in the program now because of the advantages each might have in future developments of the viscous analysis method. Green's method is capable of continuing the calculation beyond the trailing edge to determine the thickness of the wake. It is planned to examine at a later time the effects of a finite thickness wake and of the merging of the boundary layers and/or wakes from the two airfoil elements on the results of the program, especially for configurations where the elements are closely spaced. In cases where the interaction of the merging shear layers is strong integral methods may become inaccurate and the use of Bradshaw's finite difference method may be required.

The boundary layer computation provides the distribution of displacement thickness and skin friction over the airfoils. The latter is integrated to give the skin friction drag on the airfoil configuration. Following the approaches taken in the theoretical methods of analysis for single-airfoil transonic flows and multi-element incompressible flows, the major effect of the boundary layer on the inviscid flow is through weak displacement effects. Thus a correction to the inviscid solution can be obtained by allowing for an appropriate mass flow at the airfoil surface (Ref 15).

These procedures are uniformly valid in regions where the surface geometry is smooth and the inviscid surface pressures are regular. But in regions of strong interactions, such as trailing edges and shocks, ordinary boundary layer theory breaks down. In these regions, semi-empirical corrections are made to compute the displacement effects. At shock waves the computed pressure is smeared over a few mesh points. Hence, in such a region, the boundary layer will thicken considerably without separating, allowing the boundary layer computation to proceed. Sometimes the pressure rise through the shock is so large that the smearing will not prevent separation. At trailing edges the displacement thickness is extrapolated from upstream to represent a smooth streamline passing over the trailing edge. The local trailing edge solution given by Melnik, Chow and Mead (Ref 7) provides a much better model.

3.2 COUPLING OF INVISCID FLOW AND BOUNDARY LAYER

Lighthill (Ref 15) showed that the effect of the boundary layer on the outer inviscid flow over a surface is equivalent to that of a distribution of sources on the surface whose strength at any station is given by

$$v_s = \frac{1}{\rho} \frac{\partial}{\partial s} (\rho u \delta^*) \tag{12}$$

where δ^* is the displacement thickness of the boundary layer, ρ is the density and u the tangential velocity at the edge of the boundary layer. The Neumann problem for the inviscid flow discussed in the previous section is now solved subject to the boundary conditions:

$$v = v_s \text{ on } r = 1 \text{ and } r = r_s \tag{13}$$

The solution for the viscous flow is then obtained by solving iteratively for the outer inviscid flow and the boundary layer. An initial guess of zero is usually taken for the source strength, v_s. This value is updated after each boundary layer computation. Since separation is a frequent problem in multi-element airfoil systems (especially on concave surfaces near the entrance of a slot), a crude separated flow model has been incorporated into the program to enable it to run to completion. However, results in cases where the model is implemented are not necessarily accurate.

3.3 VISCOUS FLOW COMPUTATIONS

The method has been applied to a variety of two-element airfoil configurations and a few typical results are presented here. In order to evaluate the performance of the method, independent of the particular strong interaction models and possible wind tunnel blockage corrections, an essentially incompressible case is considered first. Figure 12 shows the computed and measured (Ref 16) surface pressure distributions on an NACA 23012 airfoil with a 2H flap. The plot depicts the inviscid calculation, the viscous interaction calculation, and the wind tunnel data. The computed boundary layer growth on the main airfoil surface is small. On the flap upper surface, a separated flow region occurs which has a large effect on the lift. The agreement with experimental data is excellent except in the vicinity of the leading edge of the flap. The discrepancies in this region are possibly due to slight differences between the geometry of the configuration tested and that modeled by the computation. The wind tunnel model has a long lip extending from the trailing edge of the main airfoil. This protuberance, whose length is about 5% of the chord, was used to seal off the slot when the flap was retracted and reached over the leading edge of the flap, when it was extended. The conformal mapping method used in the computation cannot handle this geometric complexity. However, the modeled geometry, as shown in Fig. 12, seemed to produce quite acceptable results over most of the configuration.

Little transonic data on airfoils with leading edge slats is available, and, as in the previous case, these configurations have regions of separated flow. In Fig. 13, the computed pressure distribution and the experimental data (Ref 17) for an NACA 64A010 airfoil with a slat at $M_\infty = 0.7$, $\alpha = 6°$ and Re = 7.8 million are compared. Lower surface separation on the slat drastically alters the flow through the slot, and again substantial discrepancies occur near the leading edge of the downstream element (for this case the main airfoil). The method predicted separation near the lower corner of the slat (which has been rounded slightly), but no attempt was made to model the massive separation region on the concave surface of the slat. Separation was also predicted on the upper surface of the slat, near the leading edge. On the main airfoil, away from the leading edge (slot) region agreement with the data is satisfactory with the shock wave predicted in approximately the correct location.

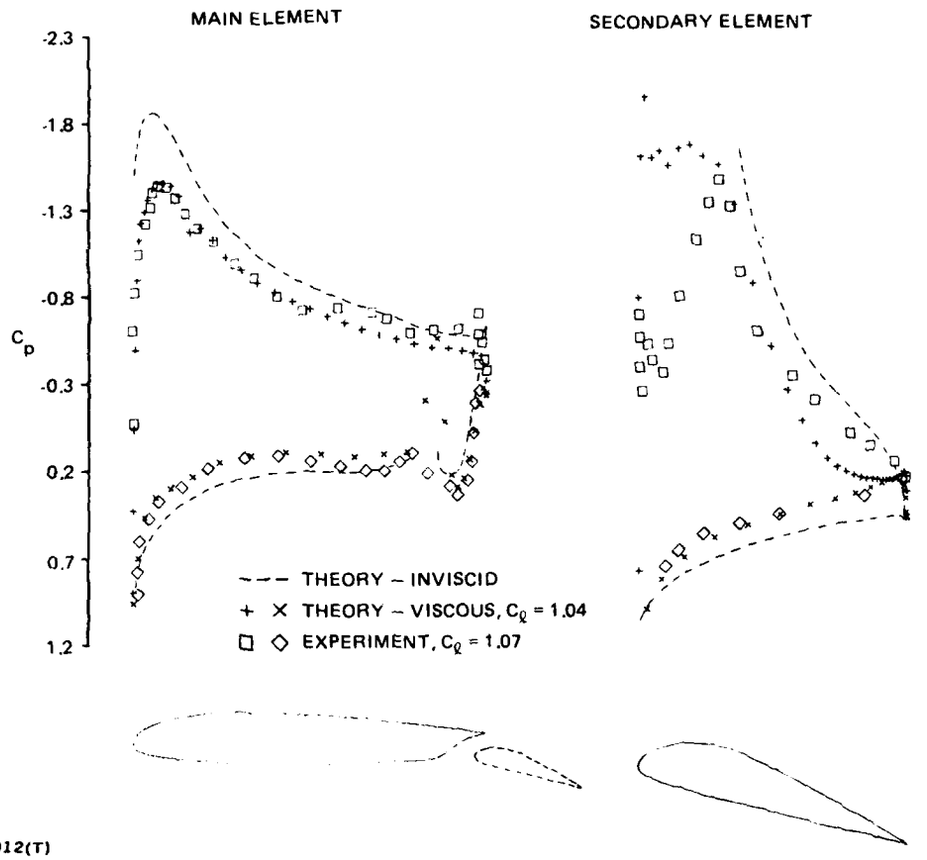

0737-012(T)

Fig. 12 Computed and Experimental Surface Pressure Distributions: NACA 23012 Airfoil With 2H Flap, $M_\infty = 0.133$, $\alpha = 0°$, $Re = 3.5 \times 10^6$

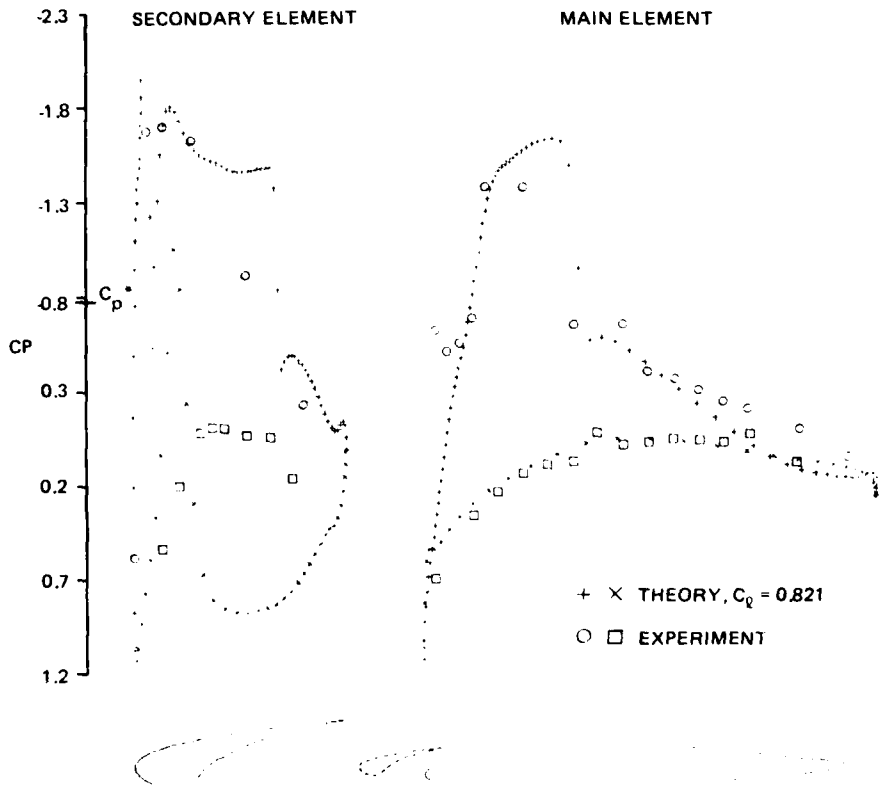

0737-013(T)

Fig. 13 Computed and Experimental Surface Pressure Distributions: NACA 64A010 Airfoil With 18A Slat; $M_\infty = 0.7$, $\alpha = 6^\circ$, $Re = 7.8 \times 10^6$

The configuration shown in Fig. 14 was obtained from a basic NACA 64A406 airfoil (Ref 5). The geometry of the system reduces to this profile when the slat is retracted except for an opening on the lower surface. The flow separation on the slat does not affect the flow coming out of the slat as much as it did in the previous case. The slenderness of the slat in this case reduces the size of the separation regions. The pressure distribution on the main airfoil is predicted quite well, including the multiple peaks near the leading edge. Figure 15 shows the Mach number contours for this case. It is interesting to note the pocket of supersonic flow existing in the slot. The exit of the slot is essentially sonic with the flow quickly reaccelerating to supersonic velocities behind it. This pattern is reflected in the multiple peaks in both the computed and experimental pressures.

Figure 16 gives the computed results and the data for the same airfoil system with the slat moved forward, thus increasing the gap size between the two elements. Again there is evidence of lower surface separation on the slot, but not to the same extent as in the previous case where the slat was further back. With less separation, in this case, agreement between data and theory on the slat is improved. The expansion into the shock on the airfoil is overestimated although the initial spike on the nose in the pressure profile is well predicted. The computed Mach number contours for this case are depicted in Fig. 17. Figure 18 gives the result for a third position of the slat, which is moved down and rotated counterclockwise with respect to the last case. Agreement between computed and experimental results is again quite good, on the main airfoil element. Separation on the slat on the lower surface and on the upper surface near the leading edge can explain the discrepancies observed here.

The wide range of applicability of the method is demonstrated by the results given for the airfoil-flap configuration in Fig. 19. This is in fact the first supercritical airfoil developed by Whitcomb (Ref 18), and the calculations are the first for this airfoil system. The two airfoil elements are very close and there is a large overlap. Also, the aft portion of the main airfoil is highly loaded as is the entire flap, a characteristic retained in the later single piece supercritical airfoils. All the features of the flow are well predicted and overall agreement is good, again with the exception of the slot exit region.

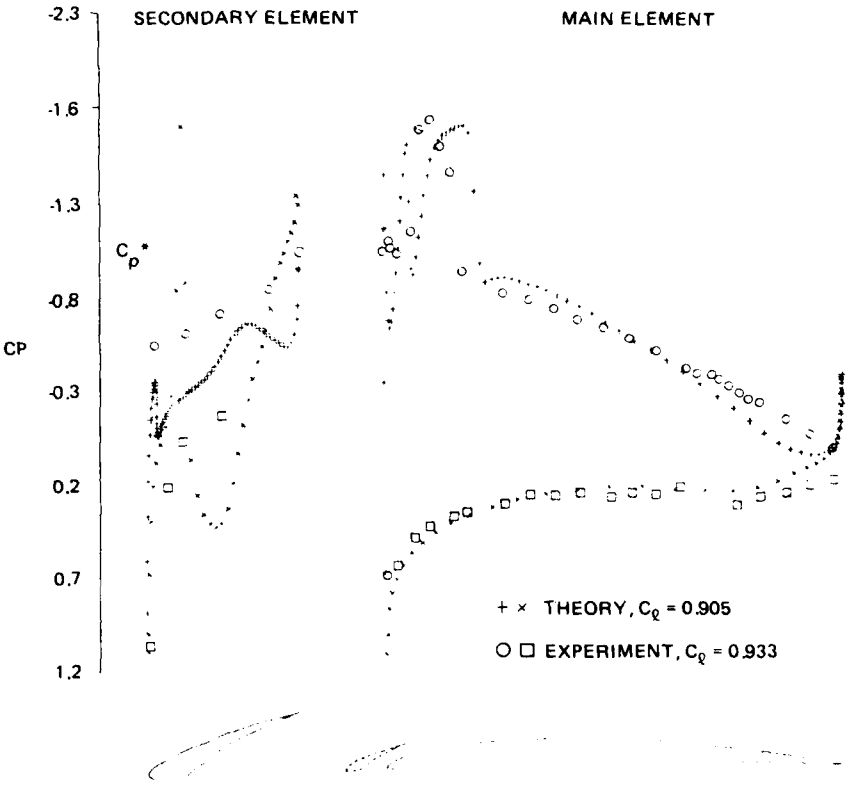

0737-014(T)

Fig. 14 Computed and Experimental Surface Pressure Distributions: NACA 64A406 Airfoil With 7.8A Slat; $M_\infty = 0.649$, $\alpha = 4.6^\circ$, Re = 2.0×10^7

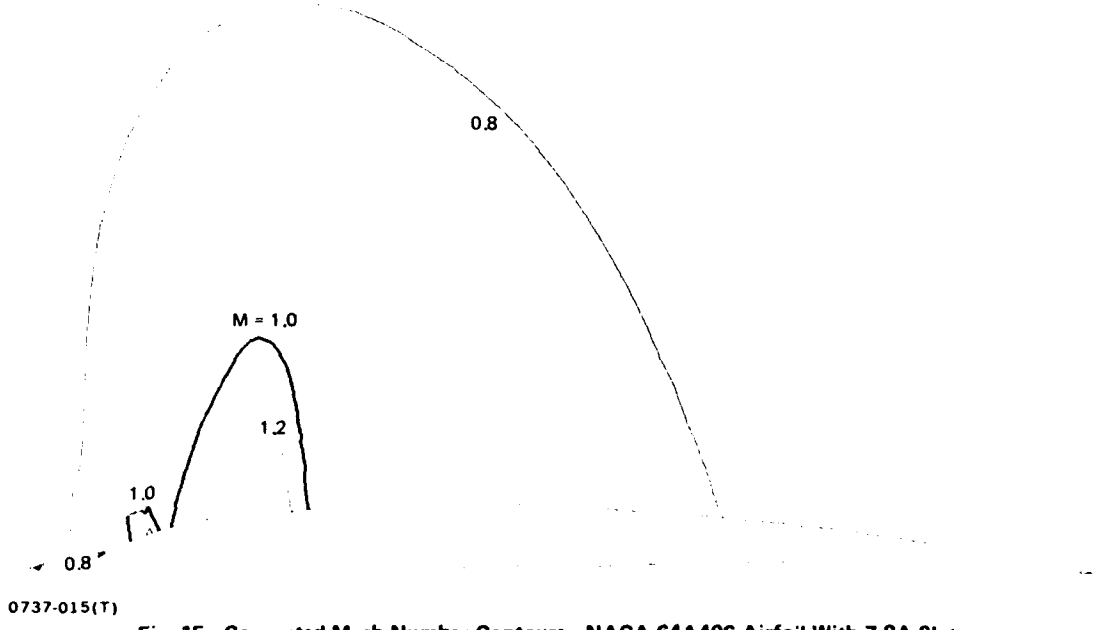

Fig. 15 Computed Mach Number Contours: NACA 64A406 Airfoil With 7.8A Slat; $M_\infty = 0.649$, $\alpha = 4.6^\circ$, $Re = 2.0 \times 10^7$

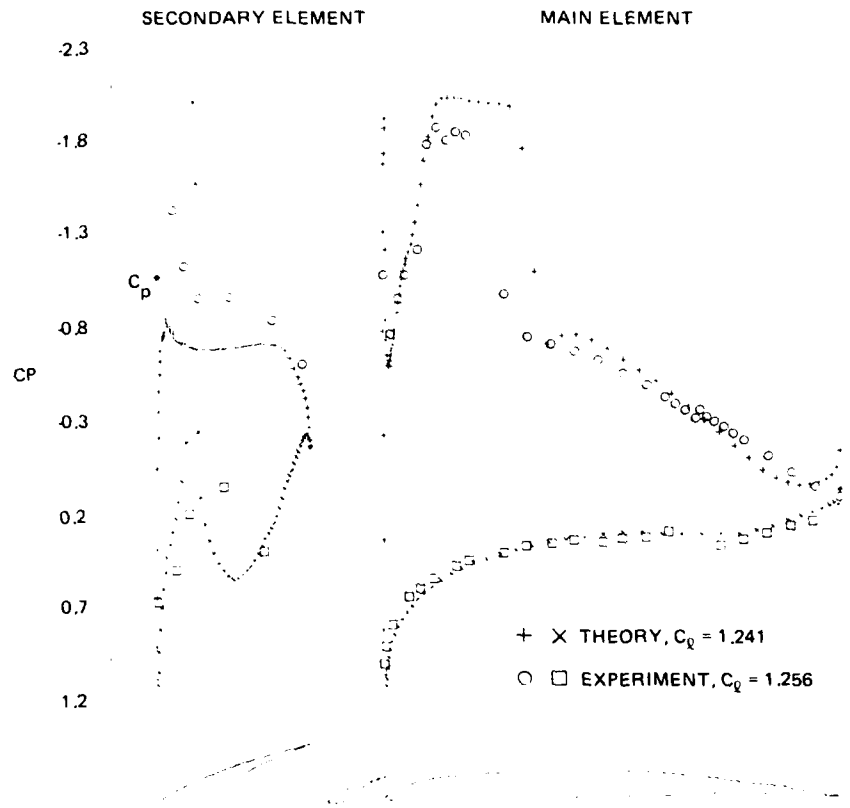

0737-016(T)

Fig. 16 Computed and Experimental Pressure Distributions: NACA 64A406 Airfoil With a 7.8F Slat; $M_\infty = 0.649$, $\alpha = 6.5^\circ$, $Re = 2.0 \times 10^7$

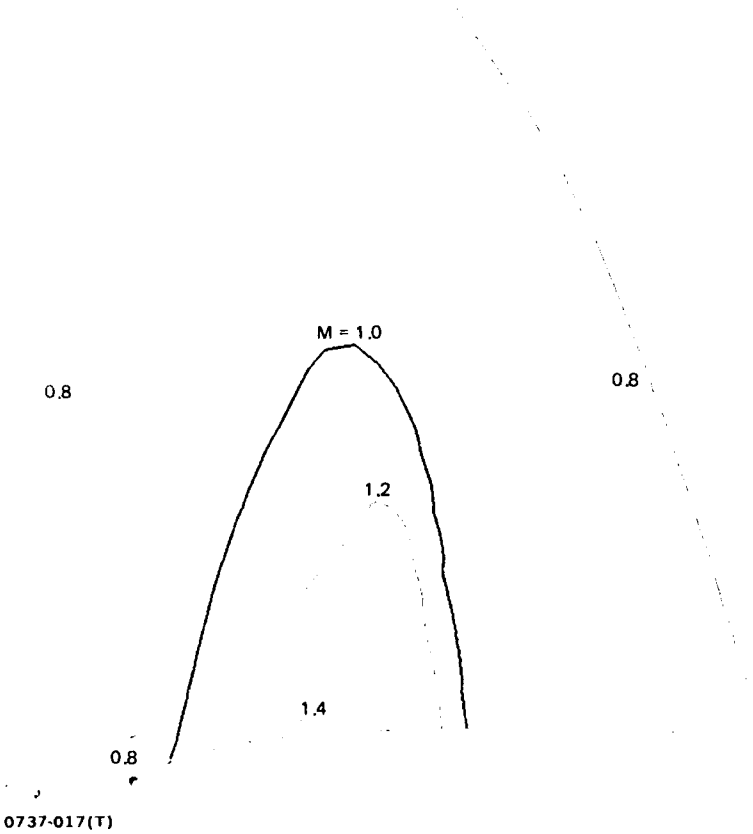

Fig. 17 Computed Mach Number Contours: NACA 64A406 Airfoil With 7.8F Slat; $M_\infty = 0.649$, $\alpha = 6.5^\circ$, $Re = 2.0 \times 10^7$

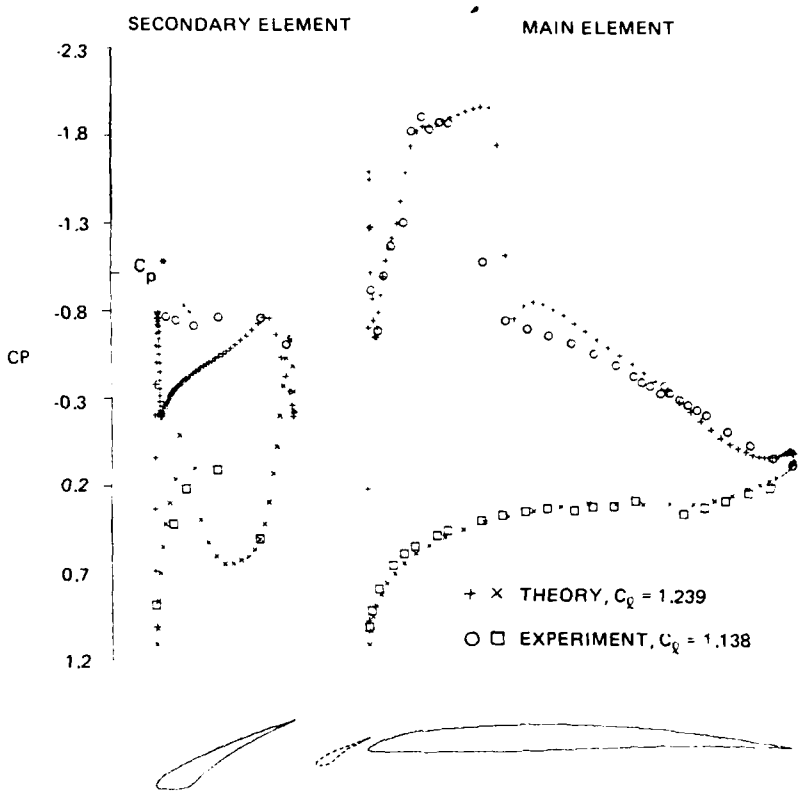

0737-018(T)

Fig. 18 Computed and Experimental Surface Pressure Distributions: NACA 64A406 Airfoil With 10.6C Slat; $M_\infty = 0.649$, $\alpha = 6.5°$, $Re = 2.0 \times 10^7$

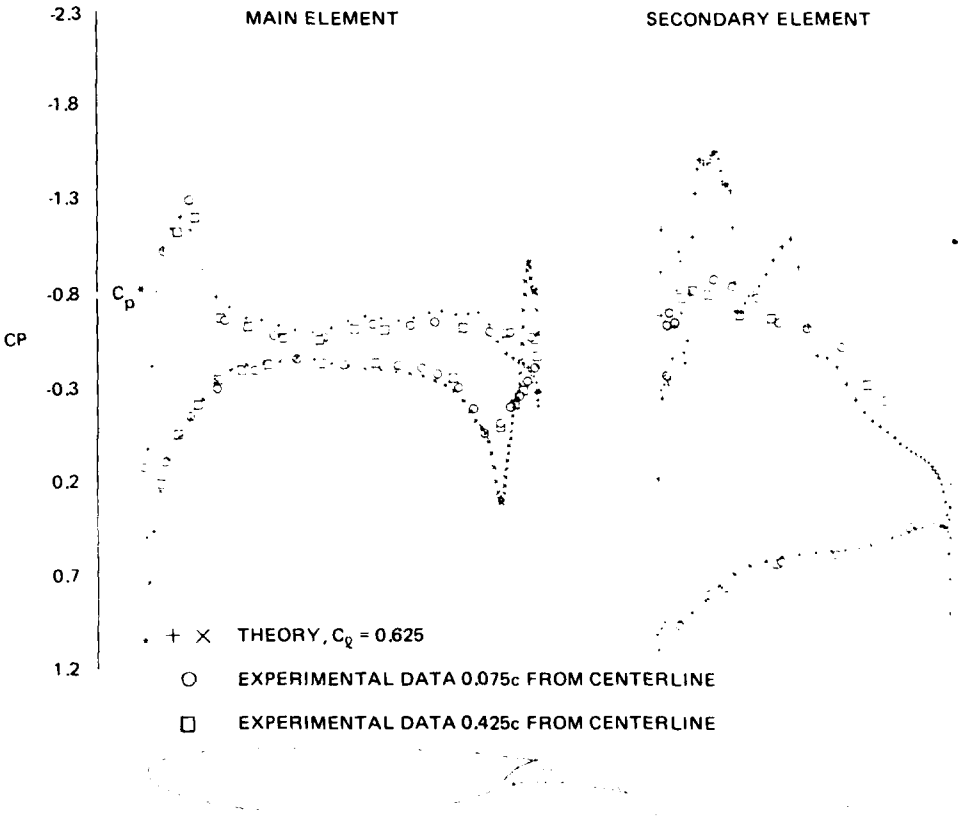

0737-019(T)

Fig. 19 Computed and Experimental Pressure Distributions: Supercritical Airfoil One, $M_\infty = 0.70, \alpha = -1.74^\circ$, $Re = 10^7$

All the calculations have been done at the Mach number and angle of attack quoted for the data by the experimenters. Thus, the possible influence of wind tunnel blockage and flow angularities was not taken into account. Not unexpectedly, the comparisons with data have been marred by the presence of substantial regions of separation. But the reason for undertaking this study was to develop a method that would help in the design of transonic maneuvering devices, and hopefully a good design would eliminate, or at least mimimize, the extent of flow separation. The present method can be used to infer the degradation in performance due to separation. The generally poor agreement between data and theory locally near a slot exit seems to indicate that a better viscous model of the flow is needed in this region. The present semi-empirical model for the trailing edge interaction region, although globally adequate, should be replaced by the more rational model proposed by Melnik, Chow and Mead (Ref 7). It also appears that the thickness of the wake passing over a downstream element should be accounted for, as should the possible merging of the wake with the boundary layer of the downstream element.

The numerical method, as has been shown, can handle an arbitrary two-element airfoil configuration. The computed results presented here were obtained on a series of three grid distributions, with a fine mesh of 120 circumferential points by 58 radial points in the mapped domain. A typical supercritical case requires about 40 minutes of computing time on an IBM 370/168 computer. The computer code is far from being optimized and computational efficiency can be improved. The most time consuming portion of the method is the solution of the inviscid flow by relaxation methods. Recently developed techniques can achieve convergence to a solution in computing times much shorter than those required by relaxation. They will be discussed in Section 5.

4. THE INVERSE DESIGN PROBLEM

The approach to the design of two-element airfoils described in this section is an extension of the procedure used in the single-airfoil problem (Ref 19,20). A difficulty with inverse design methods is that no correct formulation of the inverse problem has yet been given for compressible flow even for the single-airfoil case. Lighthill (Ref 21) showed, for the single airfoil problem, that in incompressible flow the inverse design problem is properly posed only if the desired velocity distribution satisfies three closure conditions. Two of these conditions imply that the trailing edge should be closed. The third condition implies that the free stream speed cannot be specified independently of the surface speed distribution. Lighthill was able to express these conditions in closed form and showed how, by the introduction of three adjustable parameters into an arbitrarily specified speed distribution, a solution could be obtained in every case. No closed form expression of the three constraints has been found for the inverse problem in compressible flow, but the existence of these constraints is deduced from the fact that the incompressible problem is a special case of the compressible problem. Failure to satisfy the first two constraints results, in general, in an airfoil shape with an open trailing edge. Failure to satisfy the third condition precludes the existence of any solution. In a numerical computation scheme this nonexistence of a solution appears as a convergence problem. Acceptable solutions can be attained, however, if the desired pressure distributions are obtained by making "small" modifications to pressure distributions generated from direct solutions. The consequences of violating the third constraint in these situations appear to be minor and the method described here (and also in Ref 19 and 20) is confined to such problems. This class of methods fails completely when more general pressure distributions are prescribed. Research recently completed has led to a method by which, as in the incompressible case, the single-element inverse problem can be solved in every case by introducing free parameters in an arbitrary target speed distribution. Although this method is to be extended to the two-element case, the design procedure described in this section operates under the limitations discussed above. Nonetheless, the procedure can handle meaningful design cases, as will be shown.

The "simple" design problem in which the pressure distribution is specified on both bodies and the shape of both airfoil elements is sought is only one of several possible design problems that can arise in two-element systems. In the terminology of James (Ref 22) one can also have the simply-mixed design problem, in which the pressure distribution is specified for one element and the shape is prescribed for the other. Also possible is the multiple-mixed design problem, in which either pressure or shape are prescribed piecewise on either body. The two latter problems require the solution of mixed type boundary condition problems, which entail some additional difficulties.

4.1 FULL DESIGN FORMULATION

The description of the inverse procedure is restricted initially to the "simple" design problem. Modifications to the method in the case of a mixed design case are addressed later. The procedure requires that an initial configuration be prescribed. This initial configuration provides boundaries on which the desired velocity distribution can be imposed and also an approximate metric function for the computation of the flow in the annulus. These initial boundary profiles are not required to be streamlines; in fact, the desired contour is assumed to be given by some neighboring streamline. An iteration is obviously required to make the airfoil boundary a streamline of the flow. As mentioned earlier, the present approach is restricted to cases where the target velocity distributions are modifications of direct solutions. These target distributions are defined as functions of the azimuthal coordinate θ: $u^{(n)} = F^{(N)}(\theta; r_N)$, $N = 1,2$, with $r_1 = 1$ and $r_2 = r_s$. These velocity distributions are assumed to be the tangential velocities at the two boundaries so that a line integral about each of the two boundaries gives the two circulation constants of the flow:

$$\Gamma_1 = \frac{1}{2\pi}\int_0^{2\pi} \frac{\tilde{H}K_1}{f} F^{(1)}(\theta;1)d\theta \tag{14a}$$

$$\Gamma_2 = \frac{1}{2\pi}\int_0^{2\pi} \frac{r_s\tilde{H}K_1}{f} F^{(2)}(\theta;r_s)d\theta \tag{14b}$$

$\tilde{H}$ is the metric function corresponding to the mapping of the current estimate of the airfoil configuration. In the finite difference scheme $u^{(1)}$ and $u^{(2)}$ are given at midpoints of the mesh interval. Then, with the circulation constants known, the value of G_θ at each of these points can be found:

$$(G_\theta)^{(N)} = \Gamma_2 + \frac{r}{f}\left[HK_1F^{(N)} + (\Gamma_1+\Gamma_2)E_1(r_\infty\cos\theta - r) - \frac{r}{f}\Phi_{1_\theta}\right], \quad N=1,2 \qquad (15)$$

Integration of these functions along each boundary gives the value of the potential at each grid point on the boundary itself. The constants of integration are such that the values of the potential at the trailing edges are the same values of the solution to the direct, Neumann, problem to the configuration. This strategy has proved to be adequate, but a series of direct and inverse flow problems becomes necessary. The potential functions obtained by integration provide the boundary conditions for the inverse, Dirichlet, problem. The same numerical scheme as in the direct problem is used to solve this problem. As part of the solution a velocity component normal to the computational boundaries, $v = v_s$, is computed there. These velocities are used to modify the airfoil shapes by a mass flow analysis near the boundary. Thus denoting by δ_i the distance by which the point (x_i, y_i) is to be shifted in a direction normal to the boundary in order for it to be on a streamline, the shift at the next grid point (x_{i+1}, y_{i+1}) will be

$$\delta_{i+1} = \frac{1}{(\rho u)_{i+1}}\left\{(\rho u)_i\delta_i + \frac{1}{2}[(\rho v)_i + (\rho v)_{i+1}](s_{i+1}-s_i)\right\} \qquad (16)$$

These δ's are computed by marching from the leading to the trailing edge on each surface of either airfoil. Initial values are supplied by a local analysis near the stagnation points. Once the new airfoil ordinates have been generated the new configuration is mapped into the annulus and a direct solution is found. A new Dirichlet problem is then set up and the process is repeated until the computed normal velocity component, v_s, is reduced below a given tolerance.

At the end of any particular inverse step, if the trailing edge points of the upper and lower surfaces of a contour do not coincide, the lower surface is rotated to achieve closure. Then on analysis of the newly-designed airfoil configuration, eventual discrepancies between the computed velocity distribution and the target give indications on how the target should be modified to maintain closure. Thus, in the present method, trailing edge closure is achieved by carrying out a sequence of inverse and direct solutions. Ideally the target velocity distribution should contain parameters that can be adjusted automatically to achieve closure. An additional parameter to account for the third constraint mentioned above should also be present to enable the design method to function even in cases where the targets are not "small" modifications of known direct solutions. However, even as formulated, the present method, which reflects the current state of the art, is quite useful as it will be demonstrated.

4.2 MIXED DESIGN

An alternate design strategy might require the re-design of only one of the airfoil elements. In such a case velocity inputs are required on only one contour, and boundary values for the reduced potential need to be generated on only one boundary. The approach parallels the one for the full design case. In the mixed design case now one of the circulation constants is fixed by the target velocity input. The other is determined by the requirement that the Kutta condition be satisfied at the trailing edge of the airfoil element which is being kept fixed. The flow field is then computed with Neumann-type boundary conditions on one boundary and Dirichlet-type on the other. Periodically, the potentials on the Dirichlet boundary have to be recomputed to reflect the latest value of the circulation constant associated with the unaltered shape. Once the relaxation process is converged, construction of the one airfoil takes place as before. The procedure again alternates between direct and inverse modes of solution to maintain trailing edge closure (by possibly altering the target velocities). Also, the direct problem provides an integration constant and an initial value of the circulation constant of the unaltered shape, which are needed to generate the Dirichlet-boundary potential from the target velocity.

4.3 EXAMPLES OF INVERSE DESIGN

Cases illustrating both design strategies are presented in this section. The target pressure distributions are generated as modifications of direct solutions. This is, however, exactly the mode by which airfoil design is done. Often in practice airfoil design is directed to the removal of some undesirable feature of the flow. The present method successfully accomplishes this.

The slat configuration shown in Fig. 20, typical for a modern day fighter design, has a considerable supersonic region when analyzed at a Mach number of 0.6 and an angle of attack of 6°. The supersonic region is seen more clearly in Fig. 21. As an exercise in two-element airfoil design it was decided to cut off the supersonic region by setting a lower limit to the pressure coefficient, as shown by the dashed line in Fig. 20. In this exercise, the slat, which is entirely in a subsonic stream, was to remain unchanged. Only the main airfoil element was to be altered. The results of the design program after one cycle are shown in Fig. 22 and 23. Figure 22 gives the new configuration along with the old one, and Fig. 23 depicts the pressure distribution computed on the new configuration, along with the desired input. As seen here the extent of the supersonic region has been reduced substantially, but there is a considerable discrepancy between the desired and the actual result. It will be remembered that the need for iteration in this approach to airfoil design was mentioned. In fact, if the design exercise is followed through two more cycles, much better results are obtained. Figure 24 compares the results of an analysis of the configuration obtained after three design cycles with the desired pressure distribution. The agreement now is quite good, and the result essentially has been achieved. The supersonic region that existed on the main airfoil has almost completely disappeared. In Fig. 25 the final two-element configuration is compared to the configuration obtained after a single design cycle. In comparing this figure to Fig. 22, one can see that a large part of the changes to the ordinates were actually achieved during the first design cycle. The changes become smaller on later cycles, almost as "fine-tuning" the shape.

To demonstrate the wide range of application of the program, it was applied to the flap arrangement shown in Fig. 26. This classical NACA

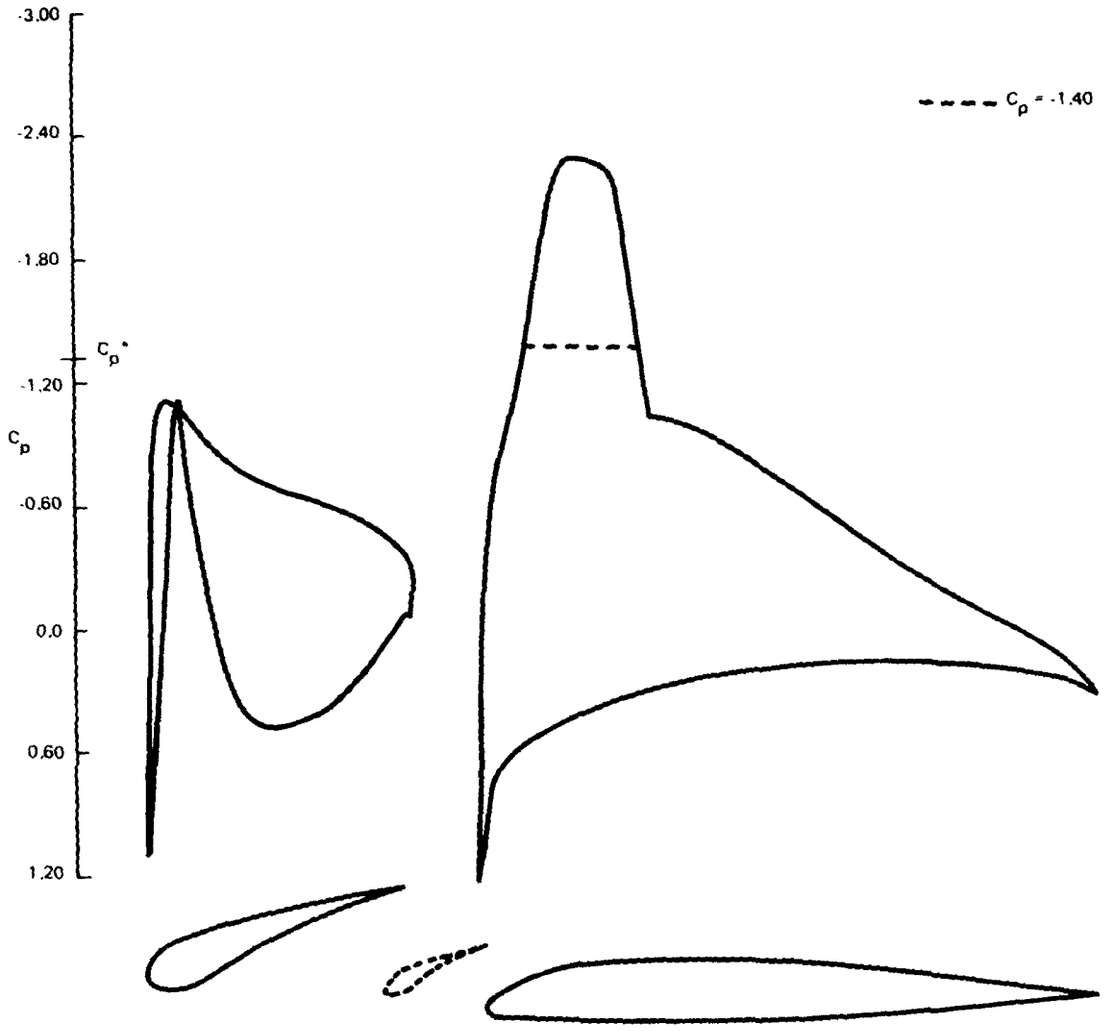

0737-020(T)

Fig. 20 Computed Pressure Distribution on Modified NACA 64A408 Airfoil with Slat; $M_\infty = 0.6$, $\alpha = 6^\circ$

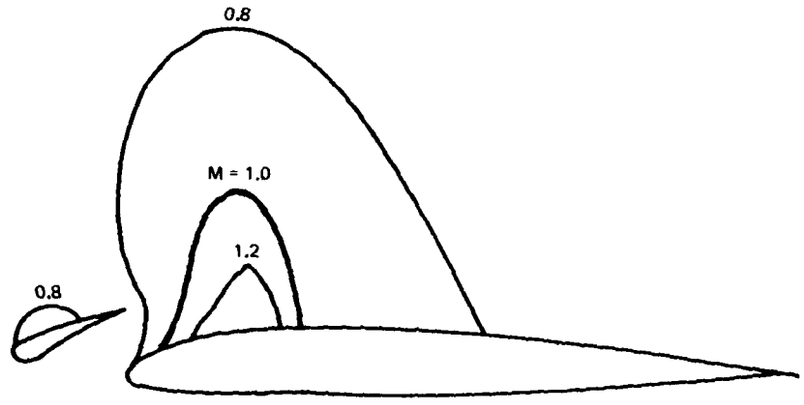

0737-021(T)

Fig. 21 Mach Number Contours on Modified NACA 64A408 Airfoil with Slat; $M_\infty = 0.6$, $\alpha = 6^\circ$

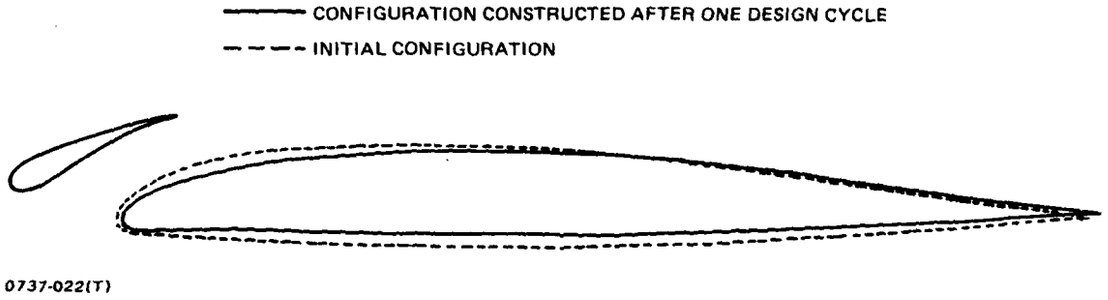

0737-022(T)

Fig. 22 Airfoil/Slat System After One Design Cycle; Main Airfoil Only Modified; $M_\infty = 0.6$

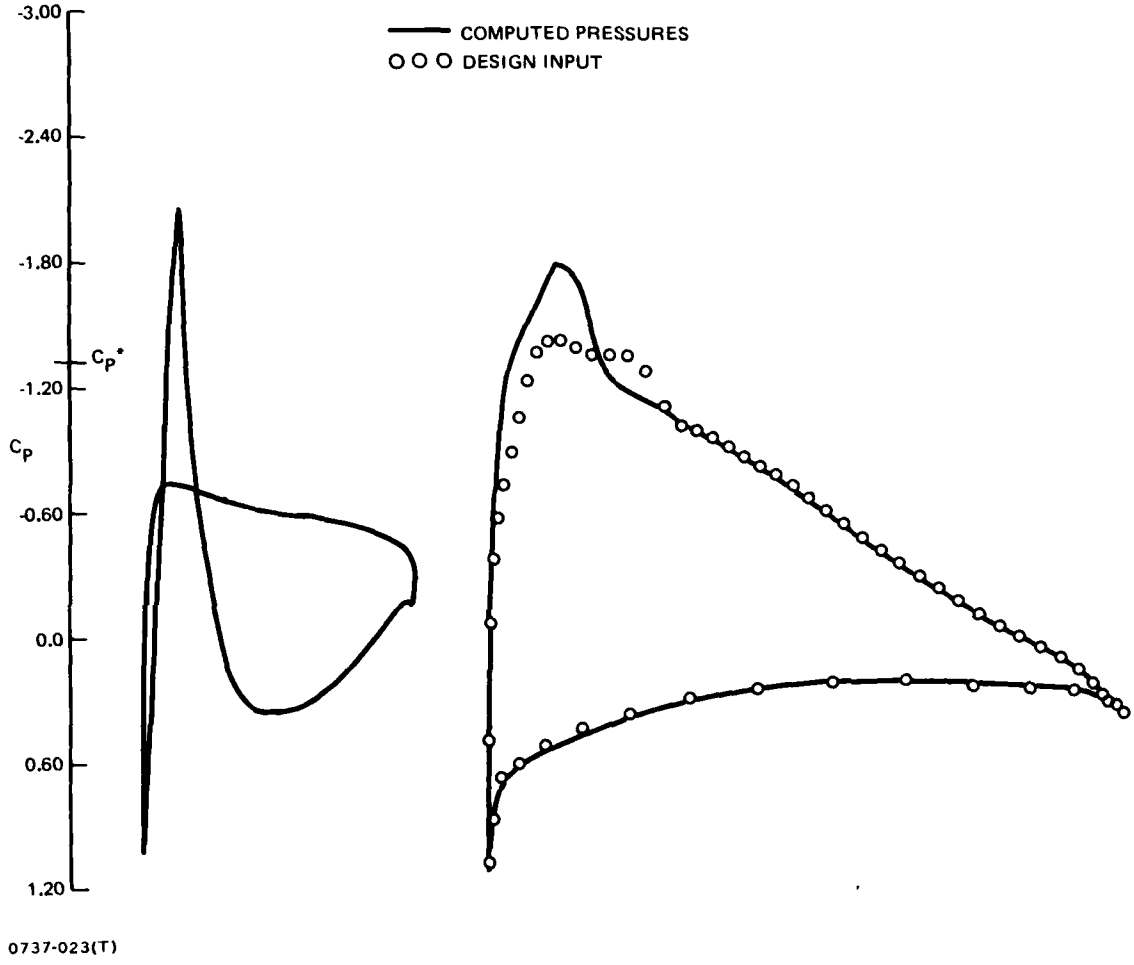

Fig. 23 Pressure Distribution Computed on Airfoil/Slat System Constructed After One Design Cycle; $M_\infty = 0.6$

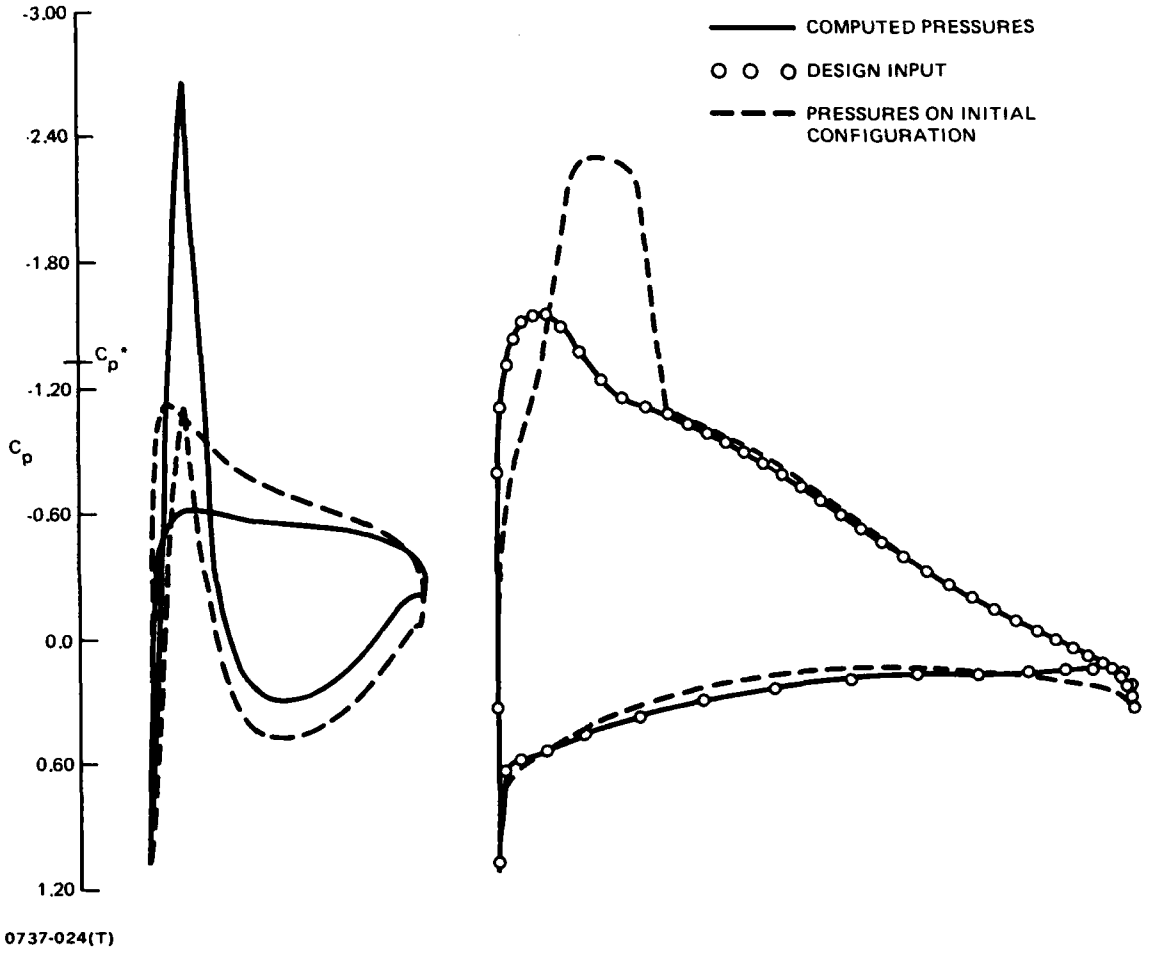

Fig. 24 Pressure Distribution Computed on Airfoil/Slat System Attained After Three Design Cycles; $M_\infty = 0.6$

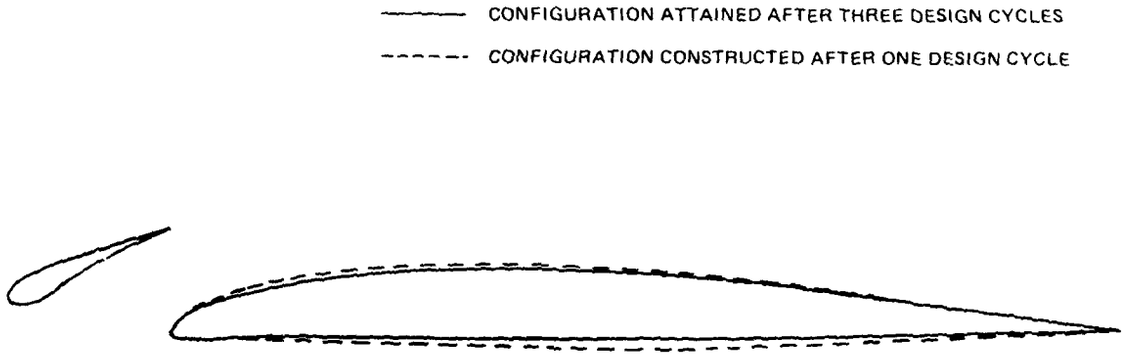

0737-025(T)

Fig. 25 Airfoil/Slat System Attained After Three Design Cycles; Main Airfoil Only Modified; $M_\infty = 0.6$

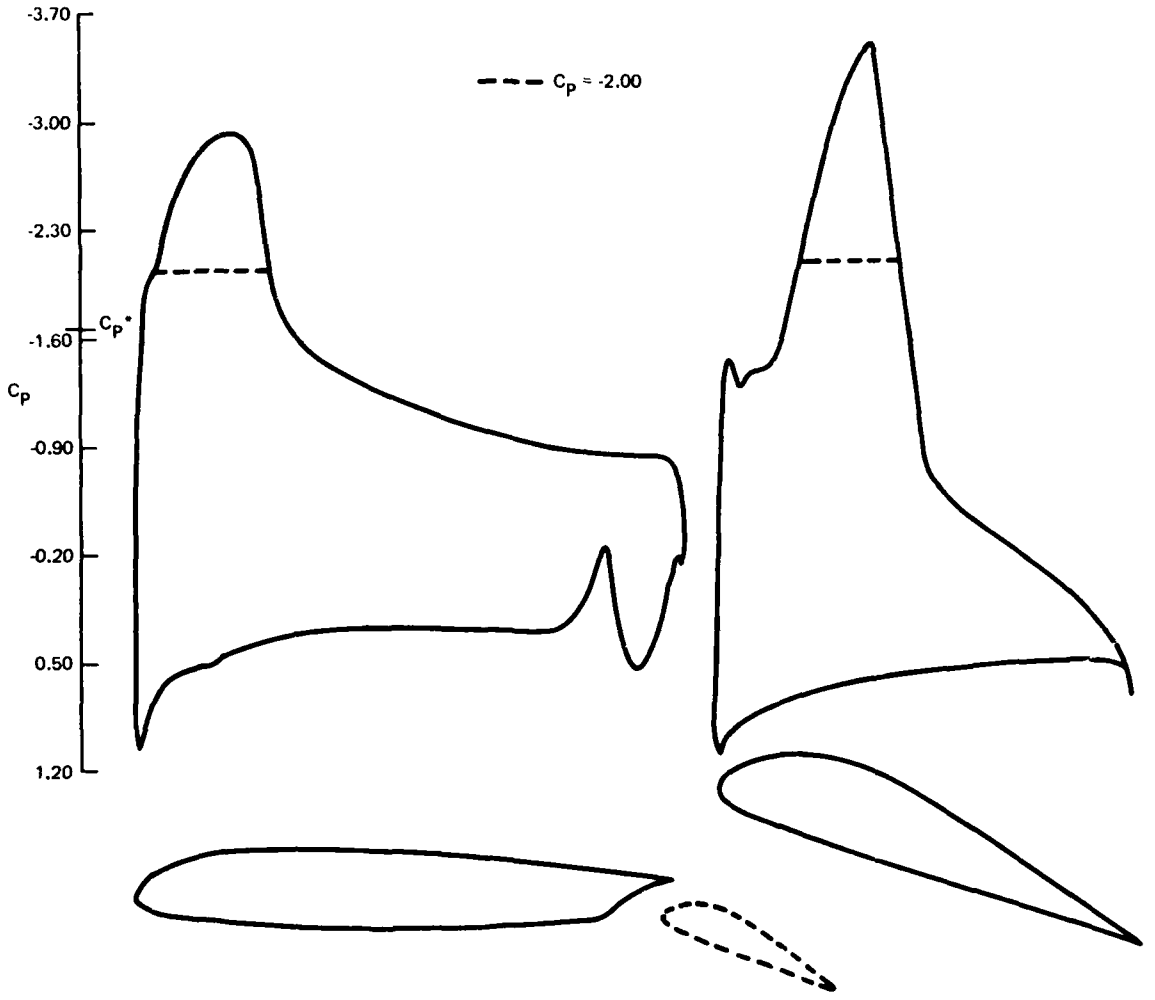

0737-026(T)

Fig. 26 Computed Pressure Distribution on NACA 23012 Airfoil With 2H Flap; $M_\infty = 0.55$, $\alpha = 0^\circ$

configuration was actually designed for low-speed applications; at a Mach number of 0.55 and an angle of attack of zero degrees, substantial supersonic regions appear over both the main airfoil component and the flap. The Mach number contour chart in Fig. 27 makes these more evident. Again, as an input to the design program, the "plateau-like" distribution given by the dashed line over the main airfoil in Fig. 26 was used. The goal was to achieve this distribution by altering only the main airfoil element. Figure 28 gives the contour achieved after one cycle, and Fig. 29 compares the computed pressure distribution actually achieved on this new configuration with the desired distribution. The result has largely been achieved after a single design cycle. However, if one looks at the flow over the flap, one sees that the supersonic region on the flap has become slightly larger with a stronger shock. Thus, while the design program achieves its goal, the actual result is not entirely desirable.

A much more interesting design goal for this configuration would be to eliminate the supersonic regions over both components, allowing both of them to be altered. This would be an example of what was called the simply-mixed design mode earlier. The results of exercising the program through one cycle in this mode are shown in Fig. 30 and 31. As seen in Fig. 31, a large expansion still exists near the leading edges of the main airfoil and the flap, although not nearly as high or as wide as on the original configuration. Because of the large interaction between the two airfoil elements and the large size of the flap, this is a much more difficult design, and the design should actually be carried out through a few more cycles. In fact, if it is followed through three more cycles, the results achieved are much better. As Fig. 32 shows, the supersonic regions have been reduced drastically, and the agreement between the desired pressure distribution and the one computed for the last configuration is very good. There is just a small discrepancy on the flap. This could possibly be eliminated if one carried out further design cycles. Figure 33 depicts the configuration obtained after four design cycles along with the one obtained after a single cycle. Figure 34 summarizes the changes made to the flap. Note that the flap trailing edge is slightly open after four cycles. This was found to be necessary by the program in order that a positive thickness be available along the entire flap chord.

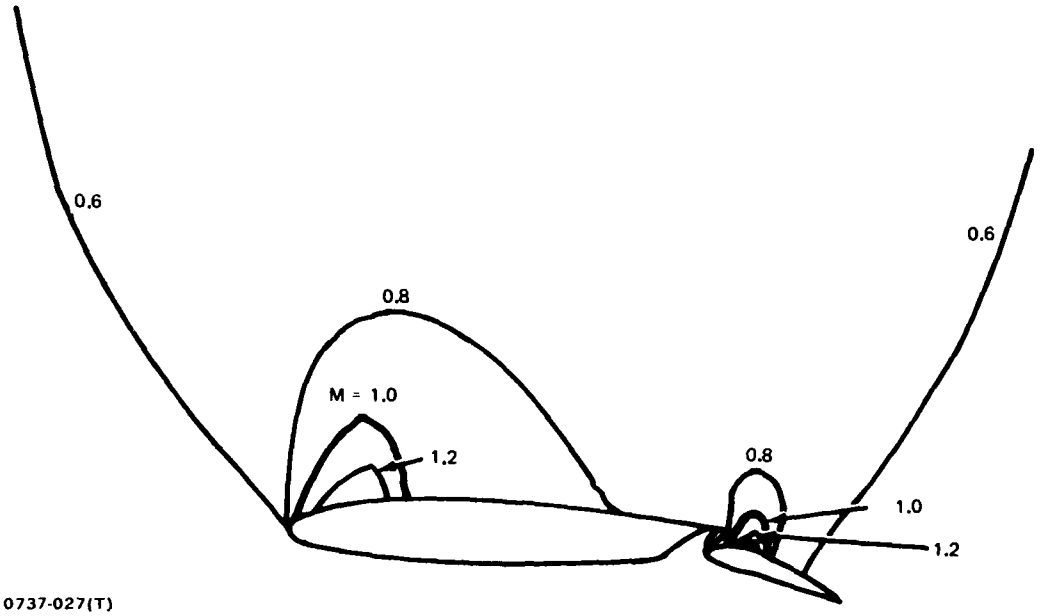

0737-027(T)

Fig. 27 Mach Number Contours on NACA 23012 Airfoil with 2H Flap; $M_\infty = 0.55$, $\alpha = 0^\circ$

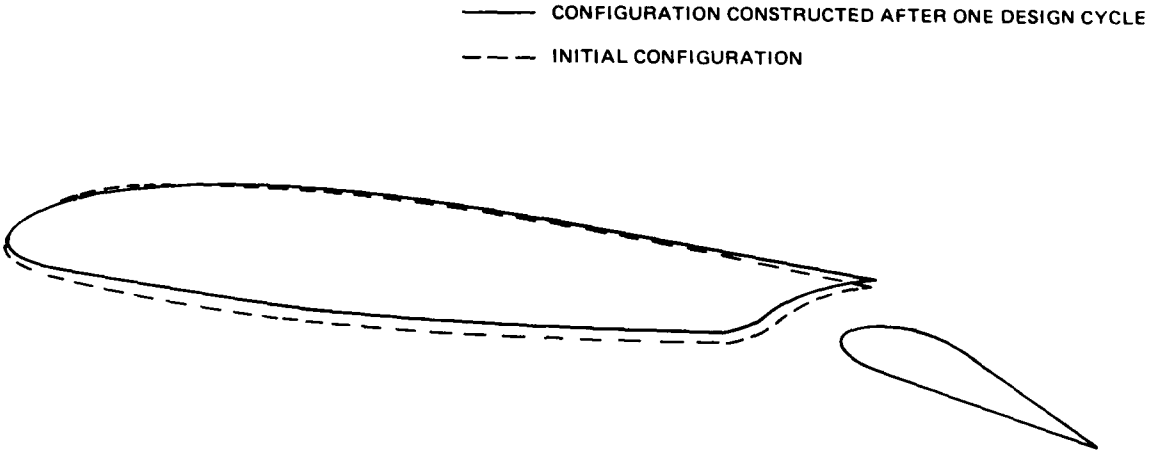

0737-028(T)

Fig. 28 Airfoil/Flap System After One Design Cycle; Main Airfoil Only Modified; $M_\infty = 0.55$

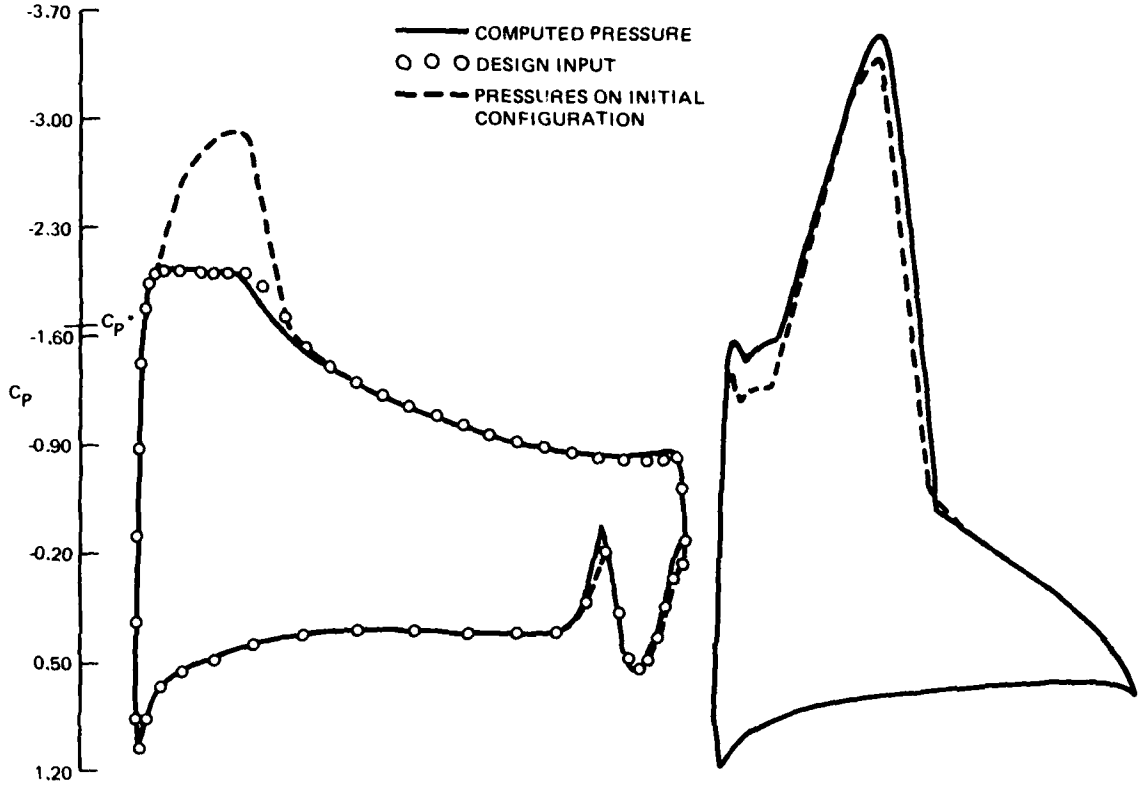

0737-029(T)

Fig. 29 Pressure Distribution Computed on Airfoil With Flap System Constructed After One Design Cycle; Main Airfoil Only Modified; $M_\infty = 0.55$

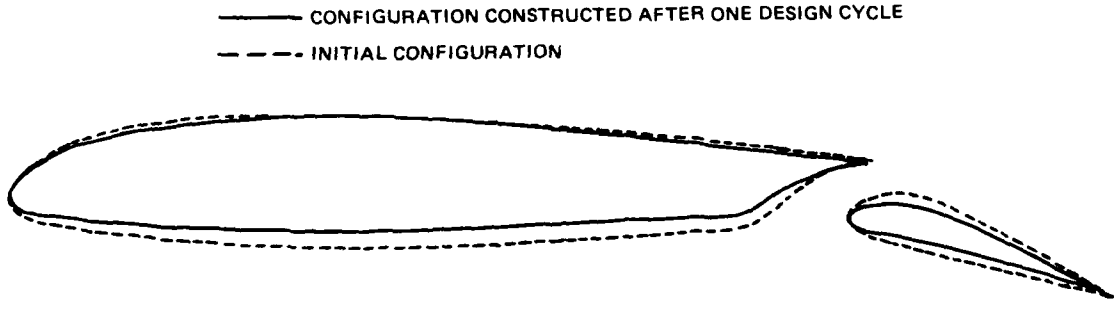

0737-030(T)

Fig. 30 Airfoil with Flap System After One Design Cycle; Both Airfoil Elements Modified; $M_\infty = 0.55$

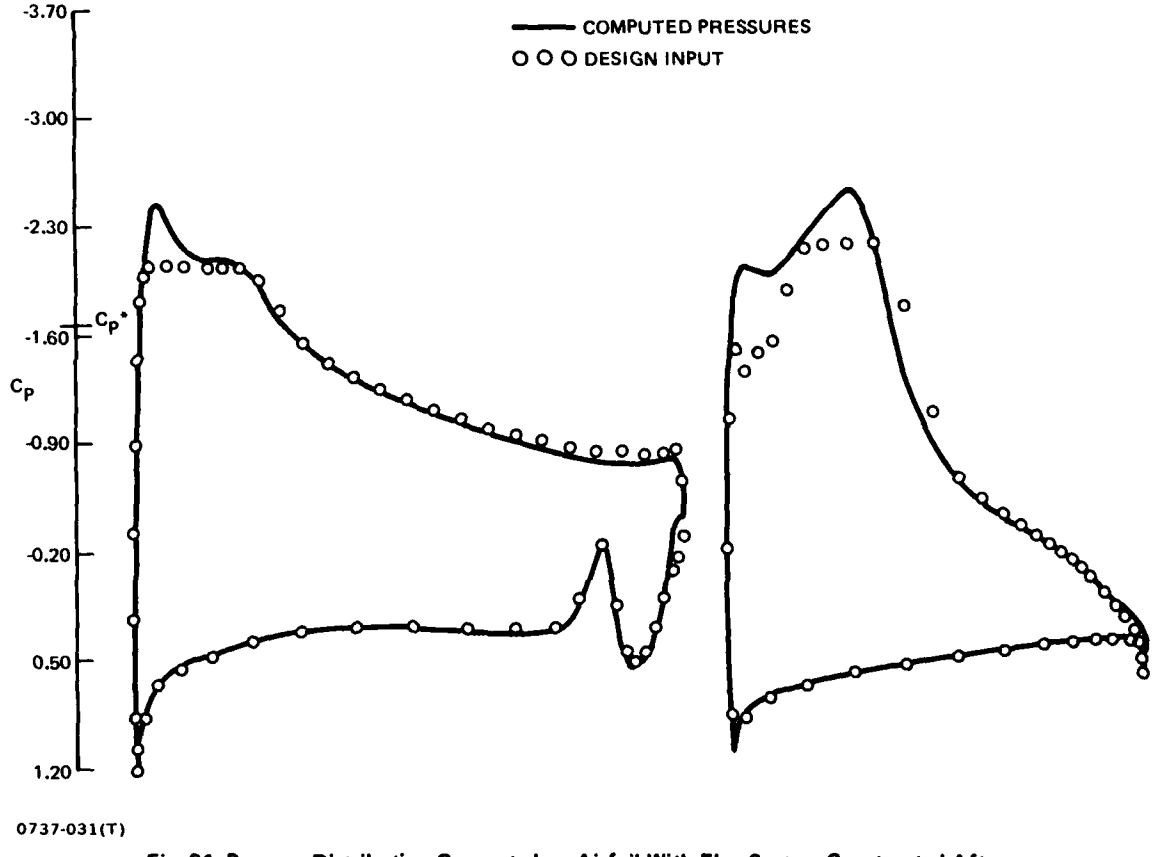

Fig. 31 Pressure Distribution Computed on Airfoil With Flap System Constructed After One Design Cycle; Both Airfoil Elements Modified; $M_\infty = 0.55$

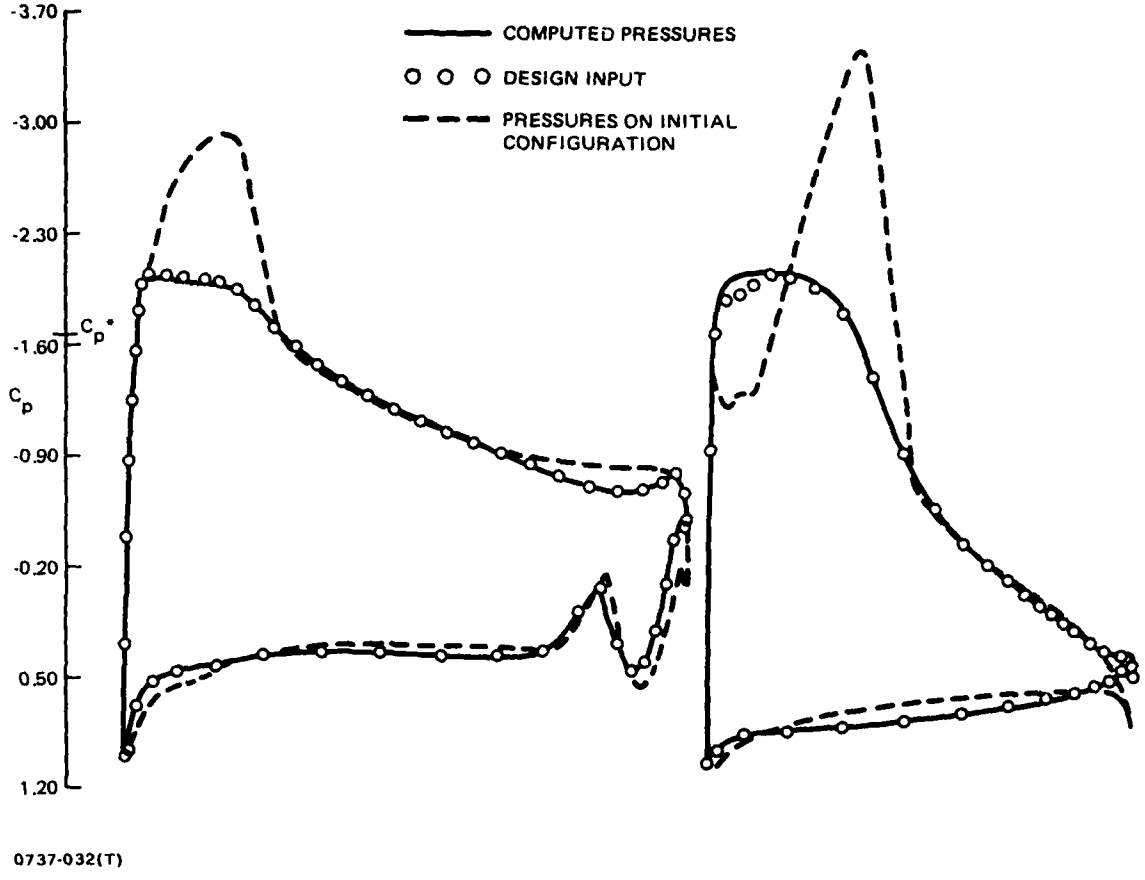

0737-032(T)

Fig. 32 Pressure Distribution Computed on Airfoil with Flap System Attained After Four Design Cycles; Both Elements Modified; $M_\infty = 0.55$

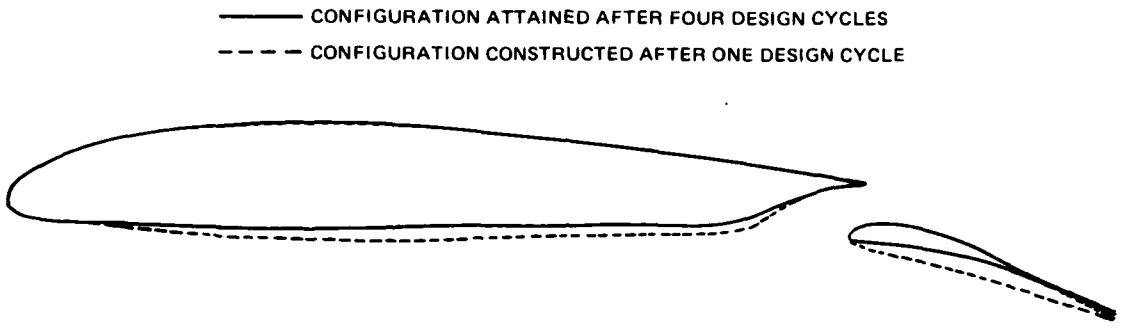

0737-033(T)

Fig. 33 Airfoil with Flap System Attained After Four Design Cycles; Both Airfoil Elements Modified; $M_\infty = 0.55$

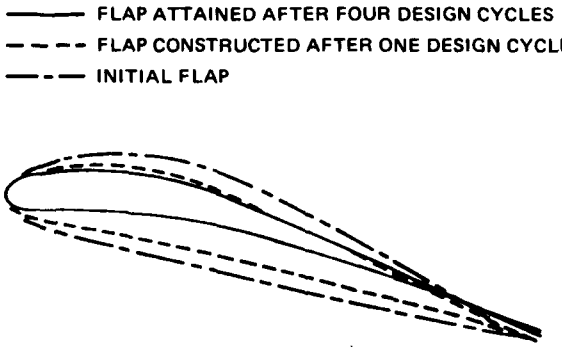

0737-034(T)

Fig. 34 Summary of Flap Geometry

5. DISCUSSION AND CONCLUSION

This study has resulted in the development of reliable computer codes for the analysis and design of two-element airfoil configurations at transonic speeds. Computations on a wide range of configurations have been shown to be in good agreement with the limited amount of data available. However, further work is required to make the theory more general.

The analysis code employs a semi-empirical theory for the trailing edge flow region. This region has been recently treated by Melnik et al. (Ref 7) more carefully. Their asymptotic analysis of this flow has led to the development of a very accurate computer program for the analysis of clean airfoils at transonic velocities. With this theory not only surface pressures but also lift and drag coefficients are predicted well. The theory can be adapted to the two-element case with some modifications. The main one involves the treatment of the wake. As in the present problem, the single-element theory of Melnik et al. uses the surface source boundary condition to account for the viscous shear layer on the airfoil. In addition, a sink distribution is placed on the wake, or rather on the coordinate line closest to the wake, to account for the wake thickness and curvature. In the single-element case, the exterior of the airfoil is mapped to the interior of a circle with infinity at the center. A radial line connecting the center of the circle to the trailing edge on the circle itself then closely approximates the wake centerline, especially just behind the airfoil where the wake effects are concentrated. In the two element case, there are no coordinate lines that approximate both airfoil wakes as Fig. 6 shows. This difficulty can be overcome by replacing the wake sink distribution with additional downwash on the airfoil surfaces.

The present program should also be generalized to take into account the possibility of shear layers from the two airfoils merging with each other, as might be the case where the two elements are very closely spaced. Low-speed high-lift systems are usually designed in such a way that the gap between the elements is the smallest possible without having merging of the shear layers. Whether this is to be done at higher speeds is still to be demonstrated. Nevertheless a computer program should be able to determine the

detrimental effects of such an occurrence if it is to find an optimum arrangement for a pair of airfoil elements. Merging can occur at the slot between the two elements, but such an occurrence is extremely rare, unless the slot is very long and the slot width is relatively small. This problem has not been treated even in the incompressible case and an investigation of the turbulence structure of such a region would need to be undertaken. A start toward such a study is given by Bradshaw in Ref 23.

A more common type merging is the mixing of the wake of the front element with the upper surface boundary layer of the rear element. Several integral methods, such as those in Ref 24 and 25, exist to treat this type of flow. These are based on velocity profiles more common on flap configurations. They are deficient in the case of the wake of a slat merging with the boundary layer of the main element. But, again, the probability of merging in the case of a slat flow is much smaller than in the case of a flap arrangement because of the former's considerably thinner wake coming off the trailing edge. Nevertheless, the slat configurations could be handled by a finite difference computational scheme similar to that in Ref 13 and described in Section 3.

As mentioned before, it would be desirable to speed up the computational scheme. Experimentation with the code has indicated that with simple eigenvalue extrapolation schemes such as those described in Ref 26 can yield reductions of 40% in the number of relaxation cycles needed to achieve a converged relaxation solution for the inviscid flow. However, the procedure is not reliable. More dramatic reductions in running times can be obtained by the use of multigrid techniques as described by Brandt (Ref 27). Arlinger (private communication), who has developed an inviscid code similar to that described in this report (Ref 28), has implemented a scheme of this type and achieved a speed-up as large as a factor of five.

Also needed are experimental data, preferably separation-free, on high-lift systems at transonic speeds. The data would be useful in verifying the analysis tools developed and in providing guidelines for future transonic maneuvering devices. Such data have recently been obtained by the author in an experimental test conducted under the sponsorship of the Office of Naval Research and will be reported on shortly.

In the area of configuration design, more basic research is required. As was shown in the examples of Section 4, the numerical procedure developed here can handle an arbitrary two-element configuration. There are no restrictions on the relative sizes of the two elements or the placement of either. Even in its present state as a pilot program it can generate remarkable results. The examples shown are really representative design cases. For while it is true that the input was a modification of a direct solution, the changes asked for were not small and the lift coefficient was changed substantially. Also this mode of configuration design - altering computed results to achieve desired flow characteristics - is very common in practice. Of course, with such a procedure the chances that a physically acceptable airfoil system actually exists are much better than they would be if the target pressure distribution was arbitrary. The procedure requires the solution of a sequence of direct and inverse problems, which can be costly in terms of computing time, and needs a man/woman in the loop to achieve trailing edge closure. This mode of operation, while acceptable, is not efficient. A method that automatically achieves trailing edge closure and can design to arbitrary pressure distributions is much more valuable. Flows with characteristics drastically different from those on present configurations could be explored. Such a method has recently been formulated for the single airfoil case. Its extension to the two-element case is to follow.

6. REFERENCES

1. Grossman, B. and Melnik, R.E., "The Numerical Computation of the Transonic Flow Over Two-Element Airfoil Systems," Proc of 5th Intern'l Conf on Numerical Methods in Fluid Dynamics, Springer-Verlag, pp 220-337, June 1976.

2. Grossman, B. and Volpe, G., "An Analysis of the Inviscid Flow Over Two-Element Airfoil Systems," Office of Naval Research Report ONR-CR215-241-1.

3. Grossman, B. and Volpe, G., "The Viscous Transonic Flow Over Two-Element Airfoil System," AIAA Paper 77-688, June 1977.

4. Volpe, G., "Two Element Airfoil Systems Designs: An Inverse Method," AIAA Paper 78-1226, July 1978.

5. Caughey, D., "An Inviscid Analysis of Transonic, Slatted Airfoils", AIAA Paper 74-541, 1974.

6. Murman, E.M. and Cole, J.D., "Calculation of Plane Steady Transonic Flows," AIAA J, Vol 9, 1971.

7. Melnik, R.E., Chow, R. and Mead, M.R., "Theory of Viscous Transonic Flow Over Airfoils at High Reynolds Numbers," AIAA Paper 77-680, June 1977.

8. Narramore, J.C. and Beatty, T.D., "An Inverse Method for the Design of Multi-Element High Lift Systems", AIAA Paper 75-879, 1975.

9. Ives, D.C., "A Modern Look at Conformal Mapping, Including Doubly Connected Regions", AIAA Paper 75-842, 1975.

10. Thwaites, B., "Approximate Calculation of the Laminar Boundary Layer," Aeron. Quart., Vol 1, 1949.

11. Rott, N. and Crabtree, L.F., "Simplified Laminar Boundary-Layer Calculations for Bodies of Revolution and for Yawed Wings", J Aeron. Sci., Vol 19, 1952.

12. Crabtree, L.F., "Prediction of Transition in the Boundary Layer on an Aerofoil," J Royal Aeron. Soc., Vol 62, 1958.

13. Bradshaw, P., Ferriss, D.M., and Atwell, N.P., "Calculation of Boundary-Layer Development Using the Turbulent Energy Equation," J Royal Aeron. Soc., Vol 28, Part 3, 1967.

14. Green, J.E., Weeks, D.J., and Broomen, J.W.F., "Prediction of Turbulent Boundary Layers and Wakes in Compressible Flow by a Lag-Entrainment Method," RAE Technical Report 72231, 1973.

15. Lighthill, M.J., "On Displacement Thickness," J Fluid Mech., Vol 4, 1958.

16. Wenzinger, D.J. and Delano, J., "Pressure Distribution Over an NACA 23012 Airfoil with a Slotted and Plain Flap," NACA Report 633, 1938.

17. Axelson, J.A. and Stevens, G.L., "Investigation of a Slat in Several Different Positions on an NACA 64A010 Airfoil for a Wide Range of Subsonic Mach Numbers," NACA TN 3129, 1954.

18. Whitcomb, R.T., and Clark, L.R., "An Airfoil Shape for Efficient Flight at Supercritical Mach Numbers," NASA TMX-1109, 1965.

19. Tranen, T.L., "A Rapid Computer Aided Transonic Airfoil Design Method," AIAA Paper No. 74-501, 1974.

20. Volpe, G., "Recent Advances in Airfoil Analysis and Design," Grumman Aerodynamics Memorandum 75-27, 1974.

21. Lighthill, M.J., "A New Method of Two-Dimensional Aerodynamic Design," ARC R&M 2112, April 1945.

22. James, R.M., "Analytical Studies of Two-Element Airfoil Systems Interim Report," Douglas Aircraft Co. Report No. MDC J5831, 1974.

23. Bradshaw, P., Dean, R.B., and McEligot, D.M., "Calculation of Interacting Turbulent Shear Layers: Duct Flow," Trans of the ASME-J of Fluids Engineering, pp 214-220, June 1973.

24. Irwin, H.P.A.H., "A Calculation Method for the Two-Dimensional Turbulent Flow Over a Slotted Flap," ARC CP No. 1267.

25. Stevens, W., Goradia, S., and Braden, J., "Mathematical Model for Two-Dimensional Multi-Component Airfoils in Viscous Flow," NASA CR-1843, 1971.

26. Caughey, D.A. and Jameson, A., "Accelerated Iterative Calculation of Transonic Nacelle Flow Fields," AIAA Paper 76-100, 1976.

27. Brandt, A., "Multi-Level Adaptive Solutions to Boundary Value Problems," Math Comp., Vol 31, pp 333-390, 1977.

28. Arlinger, B.G., "Analysis of Two-Element High Lift Systems in Transonic Flow," ICAS Paper 13, 1976.


DATE
ILME